
Grassmann Manifold Flow

Ryoma Yataka, Masashi Shiraishi

Information Technology R&D Center, Mitsubishi Electric Corporation
 5-1-1 Ofuna, Kamakura, Japan
 Yataka.Ryoma@dw.MitsubishiElectric.co.jp

Abstract

Recently, studies on machine learning have focused on methods that use symmetry implicit in a specific manifold as an inductive bias. In particular, approaches using Grassmann manifolds have been found to exhibit effective performance in fields such as point cloud and image set analysis. However, there is a lack of research on the construction of general learning models to learn distributions on the Grassmann manifold. In this paper, we lay the theoretical foundations for learning distributions on the Grassmann manifold via continuous normalizing flows. Experimental results show that the proposed method can generate high-quality samples by capturing the data structure. Further, the proposed method significantly outperformed state-of-the-art methods in terms of log-likelihood or evidence lower bound. The results obtained are expected to usher in further research in this field of study.

1 Introduction

Many machine learning algorithms aim to automatically learn and extract latent factors that explain a specific dataset. Symmetry is known to be an inductive bias (i.e., prior knowledge other than the training data that can contribute significantly to the learning results) for learning latent factors (Cohen & Welling (2016, 2017); Weiler & Cesa (2019); Satorras et al. (2021); Puny et al. (2022)). Symmetries exist in many phenomena in the natural sciences. If a target M is invariant¹ when the operation $g \in S$ designated by S applied to M , M has symmetry S . For example, a sphere remains a sphere even if a rotation R is applied; a symmetrical shape remains symmetrical even if a left-right reversal is applied.

Recently, studies have focused on methods to incorporate symmetry into models through equivariance and invariance when the data space forms a non-Euclidean space (a sphere S^n or a special unitary group $SU(n)$) (Cohen et al. (2018, 2019b); Haan et al. (2021); Graham et al. (2020); Boyda et al. (2021a)). Among them, discriminative and generative models for subspace data (e.g., shape matrices of point cloud data such as three-dimensional molecules and general object shapes, and image sets) have been proposed as viable approaches using Grassmann manifolds, which are invariant to orthogonal transformations. Numerous studies have reported their effectiveness (Ham & Lee (2008); Harandi et al. (2011); Huang et al. (2015, 2018); Souza et al. (2020); Lui (2012); Turaga et al. (2008); Fan et al. (2011); Haitman et al. (2021); Doronina et al. (2022); Souza et al. (2022)). In particular, through the application of generative models on Grassmann manifolds to inverse molecular design for shape regression and shape generation to discover new molecular structures, they can contribute to the development of drug discovery, computational anatomy, and materials science (Sanchez-Lengeling & Aspuru-Guzik (2018); Bilodeau et al. (2022)). In addition, they can contribute to the development of computer vision technologies such as video surveillance and interpolation of moving images through

¹Invariance implies the transformation π satisfies $\pi(x) = \pi(x') = \pi(g(x))$ for $x' = g(x)$ obtained by applying the operation g to the input x . The transformation π is considered invariant with respect to the operation g . A transformation π is considered equivariant with respect to an operation p if π satisfies $g(\pi(x)) = \pi(g(x))$. Invariance is a special case of equivariance wherein $\pi(g)$ is an identity transformation.

their application to the generation of a basis, which is a potential representation of video images (Garcia Satorras et al. (2021); Hong et al. (2017)).

Among the various generative models, the continuous normalizing flow (CNF) (Chen et al. (2018); Grathwohl et al. (2019); Lou et al. (2020); Kim et al. (2020); Mathieu & Nickel (2020)) is a method that has attracted attention in recent years along with the variational auto-encoder (VAE) (Kingma & Welling (2014)), auto-regressive model (Germain et al. (2015); Oord et al. (2016)), and the diffusion model (Sohl-Dickstein et al. (2015)). CNF is a method possessing theoretically superior properties that enable rigorous inference and evaluation of log-likelihood. The CNF renders the learning of extremely complex data distributions; however, no CNF has been constructed on Grassmann manifolds. Therefore, we propose a CNF on a Grassmann manifold. To construct this, we focused on the quotient structure of a Grassmann manifold and translated the problem of flow learning on a Grassmann manifold into that of preserving equivariance for orthogonal groups on a Stiefel manifold, which is its total space. The contributions of this study are as follows.

- A theory and general framework for learning flows on a Grassmann manifold was proposed. In our setting, we can train flows on a Grassmann manifold of arbitrary dimension. To the best of our knowledge, this is the first study to construct continuous normalizing flow on a Grassmann manifold in a unified approach, focusing on the quotient structure.
- The validity of the proposed approach was demonstrated by learning densities on a Grassmann manifold using multiple artificial datasets with complex data distributions. In particular, the orthogonally transformed data were proven to be correctly learned without any data augmentations by showing that un-trained transformed (i.e., rotated or mirrored) data can be generated from the trained model. Further, the model was evaluated on multiple patterns of training data and confirmed to perform well with particularly small amount of training data.
- The validity of our approach was demonstrated by its state-of-the-art performance in a molecular positional generation task.

2 Related Works

Symmetry-based Learning The concept of equivariance has been studied in recent years to leverage the symmetries inherent in the data (Cohen & Welling (2017); Cohen et al. (2019b,a); Haan et al. (2021); Finzi et al. (2020); Kondor & Trivedi (2018); Cohen et al. (2018)). In particular, early work by Cohen & Welling (2017) showed that when the data are equivariant, they can be processed with less computational cost and with lesser number of parameters. In the context of CNF (Rezende & Mohamed (2015); Chen et al. (2018); Grathwohl et al. (2019)), which are generative models, Köhler et al. (2020), Rezende et al. (2019) and Garcia Satorras et al. (2021) proposed equivariant normalizing flows to learn symmetric densities on Euclidean spaces. Further, the symmetries appearing in learning densities on a manifold were also introduced by Boyda et al. (2021b) and Katsman et al. (2021) as a conjugate equivariant flow on $SU(n)$, which is a quotient manifold, for use in lattice gauge theory. However, a normalizing flow on a Grassmann manifold capable of handling subspace data is yet to be established.

Subspace Data on the Grassmann Manifold Subspace data can be obtained on many types of data and can provide advantages such as practicability and noise robustness. For example, multi-view image set or video data (Lui (2012); Fan et al. (2011); Turaga et al. (2011); Alashkar et al. (2016)), signal data (Srivastava & Klassen (2004); Gatto et al. (2017); Souza et al. (2019); Yatake et al. (2019)), and text data (Shimomoto et al. (2021)) are often provided in the form of a set of feature vectors. Such raw data in matrix form is not very useful owing to its considerable size and noise. The analysis of its eigenspace, or column subspace, is important because alternatively, the raw data matrix can be well approximated by a low-dimensional subspace with basis vectors corresponding to the maximum eigenvalues of the matrix. Furthermore, three-dimensional shape data (Doronina et al. (2022); Haitman et al. (2021); Begelfor & Werman (2006); Yoshinuma et al. (2016)) such as point clouds are essentially represented as a subspace (shape space (Begelfor & Werman (2006); Srivastava et al. (2005); Yatake & Fukui (2017))) data on a Grassmann manifold if the scale is removed. Therefore, they inevitably give rise to the necessity of analyzing them on a Grassmann manifold.

3 Mathematical preliminaries

In this section, the basic mathematical concepts covered in this paper are described. Further details regarding the fundamentals of a Grassmann manifold are summarized in Appendix D.

3.1 Grassmann Manifold Defined as Quotient Manifold

Definition of a Grassmann Manifold A Grassmann manifold $\text{Gr}(k, D)$ is a set of k -dimensional subspaces $\text{span}(\mathbf{Y})$ (\mathbf{Y} is a matrix of k basis vectors) in the D -dimensional Euclidean space \mathbb{R}^D , and is defined as $\text{Gr}(k, D) = \{\text{span}(\mathbf{Y}) \subset \mathbb{R}^D \mid \dim(\text{span}(\mathbf{Y})) = k\}$ (Absil et al. (2008)). The $\text{span}(\mathbf{Y})$ is the same subspace regardless of a k -dimensional rotation or k -dimensional reflection applied to \mathbf{Y} on which it is spanned. In other words, $\text{Gr}(k, D)$ is a space invariant to transformations by the k -dimensional orthogonal group $\mathcal{O}(k)$. With respect to the compact Stiefel manifold $\text{St}(k, D) := \{\mathbf{Y} \in \mathbb{R}^{D \times k} \mid \mathbf{Y}^\top \mathbf{Y} = \mathbf{I}_k\}$ defined as the set of $D \times k$ -orthonormal basis matrices \mathbf{Y} , the equivalence class of $\mathbf{Y} \in \text{St}(k, D)$ determined from the equivalence relation \sim ² is defined by $[\mathbf{Y}] := \pi(\mathbf{Y}) = \{\mathbf{Y}\mathbf{Q} \in \text{St}(k, D) \mid \mathbf{Q} \in \mathcal{O}(k)\}$, where $\pi(\mathbf{Y})$ is a continuous surjection referred to as a quotient map. The equivalence class corresponds one-to-one with the k -dimensional subspace.

$$[\mathbf{Y}] = [\mathbf{X}] \iff \text{span}(\mathbf{Y}) = \text{span}(\mathbf{X}), \quad (1)$$

where $\mathbf{Y} \in \text{St}(k, D)$ is the representative of $[\mathbf{Y}]$. The quotient set composed of such $[\mathbf{Y}]$ as a whole can introduce the structure of a manifold (Sato & Iwai (2014)).

Definition 1. A Grassmann manifold as a quotient manifold is defined as follows:

$$\text{Gr}(k, D) := \text{St}(k, D) / \mathcal{O}(k) = \{[\mathbf{Y}] \mid \mathbf{Y} \in \text{St}(k, D)\}, \quad (2)$$

where $\text{St}(k, D) / \mathcal{O}(k)$ is the quotient manifold by the k -dimensional orthogonal group $\mathcal{O}(k)$ with the total space $\text{St}(k, D)$, and $\pi(\mathbf{Y})$ is the quotient map $\pi : \text{St}(k, D) \rightarrow \text{Gr}(k, D)$.

Tangent Space and Vector Field on the Grassmann Manifold Let $T_{[\mathbf{Y}]} \text{Gr}(k, D)$ be the tangent space of $[\mathbf{Y}] \in \text{Gr}(k, D)$. As the point $[\mathbf{Y}] \in \text{Gr}(k, D)$ is not a matrix, $T_{[\mathbf{Y}]} \text{Gr}(k, D)$ cannot be represented by a matrix. Therefore, treating these directly in numerical calculations is challenging. To solve this problem, we can use the representative $\mathbf{Y} \in \text{St}(k, D)$ for $[\mathbf{Y}] \in \text{Gr}(k, D)$ and the tangent vector $\xi_{\mathbf{Y}}^h \in T_{\mathbf{Y}} \text{St}(k, D)$, which is referred to as the horizontal lift of $\xi_{[\mathbf{Y}]} \in T_{[\mathbf{Y}]} \text{Gr}(k, D)$, for $\xi_{[\mathbf{Y}]}$. These facilitate computation with matrices (Absil et al. (2008)). $T_{\mathbf{Y}}^h \text{St}(k, D)$ is a subspace of the tangent space $T_{\mathbf{Y}} \text{St}(k, D)$ at \mathbf{Y} , referred to as horizontal space (i.e., the orthogonal complement of the vertical space $T_{\mathbf{Y}}^v \text{St}(k, D)$ along the geodesic composed of $\mathbf{Y}\mathbf{Q}$), and $\xi_{\mathbf{Y}}^h$ is referred to as a horizontal vector. The tangent bundle $T\text{Gr}(k, D) = \bigcup_{[\mathbf{Y}] \in \text{Gr}(k, D)} T_{[\mathbf{Y}]} \text{Gr}(k, D)$ that sums up the tangent spaces $T_{[\mathbf{Y}]} \text{Gr}(k, D)$ form vector fields $\mathbf{X} : \text{Gr}(k, D) \rightarrow T\text{Gr}(k, D)$. The conceptual diagram of the various spaces is shown in Figure 1. Further details on these concepts can be found in Appendix D.4.

3.2 Manifold Normalizing Flow

Let (\mathcal{M}, h) be a Riemannian manifold. We consider the time evolution of a base point $\mathbf{x} = \gamma(0)$, $\gamma : [0, \infty) \rightarrow \mathcal{M}$ on \mathcal{M} , whose velocity is expressed by a vector field $\mathbf{X}(t, \gamma(t))$. Intuitively, $\mathbf{X}(t, \gamma(t))$ represents the direction and speed at which \mathbf{x} moves on the curve $\gamma(t)$. Let $T_{\mathbf{x}}\mathcal{M}$ be the tangent space at \mathbf{x} and $T\mathcal{M} = \bigcup_{\mathbf{x} \in \mathcal{M}} T_{\mathbf{x}}\mathcal{M}$ be the tangent bundle. The time evolution of a point according

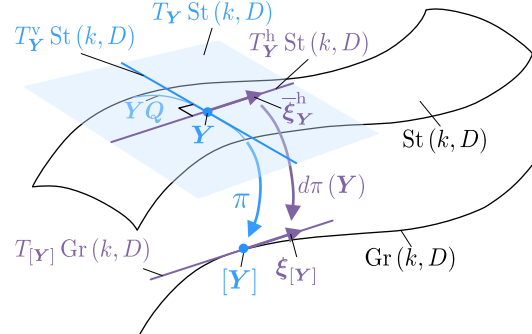


Figure 1: Conceptual diagram of spaces with horizontal lift.

²When there exists some $\mathbf{Q} \in \mathcal{O}(k)$ such that $\mathbf{X} = \mathbf{Y}\mathbf{Q}$, then \mathbf{X} and \mathbf{Y} are defined to be equivalences $\mathbf{X} \sim \mathbf{Y}$. Appendix D.2 provides further details.

to a vector field $\mathbf{X} : \mathcal{M} \times \mathbb{R} \rightarrow T\mathcal{M}$ is expressed as the following differential equation.

$$\frac{d\gamma(t)}{dt} = \mathbf{X}(t, \gamma(t)), \quad \gamma(0) = \mathbf{x}. \quad (3)$$

Let $F_{\mathbf{X},T} : \mathcal{M} \rightarrow \mathcal{M} : \mathbf{x} \mapsto F_{\mathbf{X},T}(\mathbf{x})$ be defined as the map from $\forall \mathbf{x} \in \mathcal{M}$ to the evaluated value at time T on the curve $\gamma(t)$ starting at \mathbf{x} . This map $F_{\mathbf{X},T}$ is known as the flow of \mathbf{X} (Lee (2003)).

Recently, Mathieu & Nickel (2020) introduced the Riemann CNF (RCNF), wherein the random variable $\mathbf{z}(t) \in \mathcal{M}$ is assumed to be time-dependent and the change in its log-likelihood follows the instantaneous change formula for the variable. This is an extension to the CNF (Chen et al. (2018); Grathwohl et al. (2019)) to a Riemannian manifold. Specifically, when p_θ is the density parameterized by θ , the derivative of the log-likelihood is expressed as $\frac{d \log p_\theta(\mathbf{z}(t))}{dt} = -\nabla \cdot \mathbf{X}_\theta(t, \mathbf{z}(t))$, where \mathbf{X}_θ is the vector field parameterized by θ and $\nabla \cdot \mathbf{X}_\theta$ is the divergence of \mathbf{X}_θ . By integrating this over time, the sum of the changes in log-likelihood with flow $F_{\mathbf{X},t_1\theta}$ can be computed.

$$\log p_\theta(\mathbf{z}(t_1)) = \log p\left(F_{\mathbf{X},t_1\theta}^{-1}(\mathbf{z}(t_1))\right) - \int_{t_0}^{t_1} \nabla \cdot \mathbf{X}_\theta(t, \mathbf{z}(t)) dt. \quad (4)$$

4 Invariant Densities from Grassmann Manifold Flow

This section provides a tractable and efficient method for learning densities on a Grassmann Manifold $\text{Gr}(k, D)$. However, the method for preserving the flow on $\text{Gr}(k, D)$ is non-trivial. Therefore, we derive the following implications.

1. **Vector field on $\text{Gr}(k, D)$ \Leftrightarrow Flow on $\text{Gr}(k, D)$ (Proposition 1).**
2. **Flow on $\text{Gr}(k, D)$ \Leftrightarrow Probability density on $\text{Gr}(k, D)$ (Proposition 2).**
3. **Construction of a prior probability density function for an efficient sampling on $\text{Gr}(k, D)$ (Proposition 3).**

These series of propositions show that by using a prior distribution on $\text{Gr}(k, D)$ that can be easily sampled, a flow that generates a complex probability density distribution on $\text{Gr}(k, D)$ can be obtained. We defer the proofs of all propositions to Appendix B.

4.1 Construction of Flow from Vector Field on $\text{Gr}(k, D)$

To construct flows on $\text{Gr}(k, D)$, we use tools in the theory of manifold differential equations. In particular, there is a natural correspondence between the vector fields on $\text{Gr}(k, D)$ and the flows on $\text{Gr}(k, D)$. This is formalized in the following proposition.

Proposition 1. *Let $\text{Gr}(k, D)$ be a Grassmann manifold, \mathbf{X} be any time-dependent vector field on $\text{Gr}(k, D)$, and $F_{\mathbf{X},T}$ be a flow on a \mathbf{X} . Let $\bar{\mathbf{X}}$ be any time-dependent horizontal lift and $\bar{F}_{\bar{\mathbf{X}},T}$ be a flow of $\bar{\mathbf{X}}$. $\bar{\mathbf{X}}$ is a vector field on $\text{St}(k, D)$ if and only if $\bar{F}_{\bar{\mathbf{X}},T}$ is a flow on $\text{St}(k, D)$ and satisfies invariance condition $\bar{\mathbf{X}} \sim \bar{\mathbf{X}}'$ for all $\bar{F}_{\bar{\mathbf{X}},T} \sim \bar{F}_{\bar{\mathbf{X}}',T}$. Therefore, \mathbf{X} is a vector field on $\text{Gr}(k, D)$ if and only if $F_{\mathbf{X},T} := [\bar{F}_{\bar{\mathbf{X}},T}]$ is a flow on $\text{Gr}(k, D)$, and vice versa.*

4.2 Construction of Probability Densities with Flow on $\text{Gr}(k, D)$

We show that the flow on $\text{Gr}(k, D)$ induces density on $\text{Gr}(k, D)$.

Proposition 2. *Let $\text{Gr}(k, D)$ be a Grassmann manifold. Let p be the probability density on $\text{Gr}(k, D)$ and F be the flow on $\text{Gr}(k, D)$. Suppose \bar{p} is a density on $\text{St}(k, D)$ and \bar{F} is a flow on $\text{St}(k, D)$. Then, the distribution $\bar{p}_{\bar{F}}$ after transformations by \bar{F} is also a density on $\text{St}(k, D)$. Further, the invariance condition $\bar{p}_{\bar{F}} \sim \bar{p}_{\bar{F}'}$ is satisfied for all $\bar{F} \sim \bar{F}'$. Therefore, $p_F := [\bar{p}_{\bar{F}}]$ is a distribution on $\text{Gr}(k, D)$.*

In the context of RCNF, Proposition 2 implies that the application of a flow on $\text{Gr}(k, D)$ to a prior distribution on $\text{Gr}(k, D)$ results in a probability density on $\text{Gr}(k, D)$. Thus, the problem of constructing a probability density on $\text{Gr}(k, D)$ is reduced to that of constructing a vector field on $\text{Gr}(k, D)$.

Algorithm 1 Random Sampling from $p_{\text{Gr}(k, D)}([\mathbf{X}]; [\mathbf{M}], \mathbf{U}, \mathbf{V})$

Require: A mean matrix $\mathbf{M} \in \text{St}(k, D)$, a rows covariance matrix $\mathbf{U} \in \mathbb{R}^{D \times D}$ and a columns covariance matrix $\mathbf{V} \in \mathbb{R}^{k \times k}$.

- 1: Sample a $\text{Vec}(\mathbf{Z}) \in \mathbb{R}^{Dk}$ from Gaussian Distribution $\mathcal{N}_{Dk}(\mathbf{0}, \mathbf{V} \otimes \mathbf{U})$ and reshape to $\mathbf{Z} \in \mathbb{R}^{D \times k}$.
- 2: Compute a projected horizontal vector $\bar{\xi}_M^h = (\mathbf{I}_D - \mathbf{M}\mathbf{M}^\top)\mathbf{Z}$.
- 3: Compute a representative $\mathbf{Y} = \bar{R}_M(\bar{\xi}_M^h) = \mathbf{M} + \bar{\xi}_M^h - \left(\frac{1}{2}\mathbf{M} + \frac{1}{4}\bar{\xi}_M^h\right)\left(\mathbf{I}_k + \frac{1}{4}\bar{\xi}_M^{h\top}\bar{\xi}_M^h\right)^{-1}\bar{\xi}_M^{h\top}\bar{\xi}_M^h$ of the equivalence class $[\mathbf{Y}] \in \text{Gr}(k, D)$.

4.3 Prior Probability Density Function on $\text{Gr}(k, D)$

To construct a flow on $\text{Gr}(k, D)$, a prior distribution that is easy to sample as a basis for the transformation is required, although the method for constructing such a distribution is non-trivial. This study introduced a distribution based on the matrix-variate Gaussian distribution as a prior on $\text{Gr}(k, D)$ that is easy to sample and construct a flow on $\text{Gr}(k, D)$.

Proposition 3. *The distribution $p_{\text{Gr}(k, D)}$ on a Grassmann manifold $\text{Gr}(k, D)$ based on the matrix-variate Gaussian distribution \mathcal{MN} can be expressed as follows.*

$$p_{\text{Gr}(k, D)}([\mathbf{X}]; [\mathbf{M}], \mathbf{U}, \mathbf{V}) = V_{\text{Gr}(k, D)} \mathcal{MN}\left(\bar{\xi}_M^h; \mathbf{0}, \mathbf{U}, \mathbf{V}\right) \left| \det\left(\frac{d\bar{R}_M}{d\bar{\xi}_M^h}\right) \right|, \quad (5)$$

where \mathbf{M} is an orthonormal basis matrix denoting the mean of the distribution, \mathbf{U} is a positive definite matrix denoting the row directional variance, \mathbf{V} is a positive definite matrix denoting the column directional variance, and $\bar{\xi}_M^h$ is a random sample from \mathcal{MN} in an $k(D - k)$ -dimensional horizontal space $T_M^h \text{St}(k, D)$. $V_{\text{Gr}(k, D)}$ denotes the total volume of $\text{Gr}(k, D)$ defined by (115), \bar{R}_M denotes the horizontal retraction at \mathbf{M} , and $\left| \det\left(\frac{d\bar{R}_M}{d\bar{\xi}_M^h}\right) \right|$ denotes the Jacobian.

A retraction is a map for communicating data between a manifold and its tangent bundles, and is a first-order approximation of an exponential map (Zhu & Sato (2021)). Various methods of retraction have been proposed (Absil et al. (2008); Fiori et al. (2015); Zhu & Sato (2021)); particularly, the one based on the Cayley transform, which is differentiable and does not require matrix decomposition. We use (40) as a Cayley transform based horizontal retraction. Further details are provided in Appendix D.6.

5 Learning Probability Densities with Flow

5.1 Training Paradigms

Using the results of Section 4, a flow model on a Grassmann manifold $\text{Gr}(k, D)$ is constructed. This study describes the flow model on $\text{Gr}(k, D)$ as **GrCNF**. In the proposed GrCNF, the probability density function in Section 4.3 is first constructed as a prior distribution. Subsequently, the vector field $\mathbf{X}_\theta : \text{Gr}(k, D) \times \mathbb{R} \rightarrow T\text{Gr}(k, D)$ that generates the flow model $F_{\mathbf{X}_\theta, T}$ is constructed using a neural network, wherein stepwise integration on the manifold occurs based on (4). The RCNF (Mathieu & Nickel (2020)) framework is used for integration and divergence calculations. In the integration steps, the ordinary differential equation (ODE) is solved using the ODE solver with orthogonal integration. The learnable parameters are updated using backpropagation to maximize the sum of the computed log-likelihood. Further details on our ODE solver and exact loss function can be found in Appendix C.1 and C.2.1.

5.2 Sampling Algorithm from Prior

We propose a sampling algorithm on $\text{Gr}(k, D)$ derived from the Cayley transform, based on the results of Section 4.3. The algorithm of sampling from a distribution on $p_{\text{Gr}(k, D)}$ is shown in Algorithm 1. The Vec denotes the map of vertically concatenating matrices and converting them into a vector.

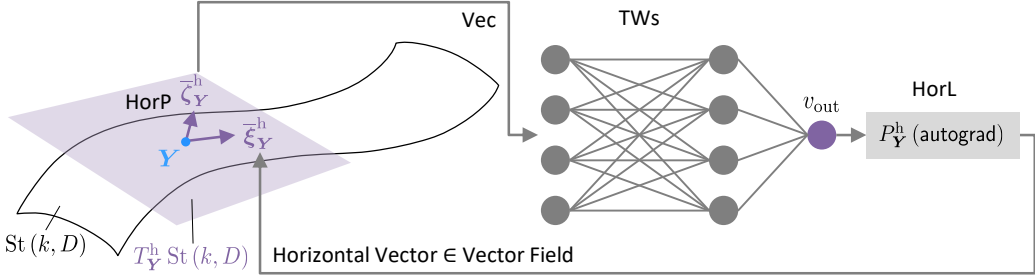


Figure 2: Conceptual diagram of the vector field calculation procedure. HorP denotes the horizontal projection layer, TWs denotes the multiple time weighted layers, and HorL denotes the horizontal lift layer. The sequence of procedure represents that, given an input of \mathbf{Y} , a horizontal vector $\bar{\xi}_{\mathbf{Y}}^h$ is obtained as a result.

5.3 Construction of Vector Field

We describe the method to construct the vector field $\mathbf{X}_\theta : \text{Gr}(k, D) \times \mathbb{R} \rightarrow T\text{Gr}(k, D)$ that generates the flow $F_{\mathbf{X}_\theta, T}$. The learnable parameters θ of \mathbf{X}_θ are feed forward neural networks, which accept the representative $\mathbf{Y} \in \text{St}(k, D)$ of $[\mathbf{Y}]$ on $\text{Gr}(k, D)$ inputs and output a horizontal lift $\bar{\xi}_{\mathbf{Y}}^h \in T_{\mathbf{Y}}^h \text{St}(k, D)$ of $\xi_{[\mathbf{Y}]} \in T_{[\mathbf{Y}]} \text{Gr}(k, D)$ that satisfies (9). The structure of the \mathbf{X}_θ is extremely important because it directly determines the ability of the distribution to be represented. To address these geometric properties, the following specific input and intermediate layers are used to obtain a $\mathcal{O}(k)$ -invariant function value v_{out} for the output layer. Subsequently, \mathbf{X}_θ is obtained by applying automatic differentiation (Paszke et al. (2017)) to v_{out} at the output layer. Figure 2 shows a conceptual diagram of procedures for vector field calculation.

Input Layer The input layer maps the input representative \mathbf{Y} to a point $\bar{\xi}_{\mathbf{Y}}^h$ in the horizontal space $T_{\mathbf{Y}}^h \text{St}(k, D)$. The tangent space is $T_{\mathbf{Y}}^h \text{St}(k, D) \cong \mathbb{R}^{(D-k) \times k}$ because it is a linear space (Absil et al. (2008)). A horizontal projection $\text{HorP} : \text{St}(k, D) \rightarrow \mathbb{R}^{(D-k) \times k}$ is constructed as an input layer.

$$\text{HorP}(\mathbf{Y}) = (\mathbf{I}_D - \mathbf{Y}\mathbf{Y}^\top) \mathbf{W}, \quad (6)$$

where \mathbf{W} is the weight. HorP is an orthogonal projection to a horizontal space $T_{\mathbf{Y}}^h \text{St}(k, D)$ on $\text{St}(k, D)$ at \mathbf{Y} , with the ability to project \mathbf{W} onto horizontal space, that is, to obtain a representation of \mathbf{Y} on horizontal space.

Intermediate Layer To model the dynamics over horizontal space, intermediate layers based on neural networks are constructed. The intermediate layers are particularly important for the power to represent the distribution, and although various configurations are possible, we specifically employ a time weighted TW layer, a function that weights with time evolution.

$$\text{TW}(\mathbf{x}, t) = (\mathbf{W}\mathbf{x} + \mathbf{b}) \sigma(t), \quad (7)$$

where \mathbf{W} and \mathbf{b} are the weight and the bias, $\sigma(\cdot)$ denotes the sigmoid function. The TL layer can be stacked multiply, and the overall power of expression increases with increase in the number of layers. The input \mathbf{x} of first intermediate layer is $\mathbf{x} = \text{Vec} \circ \text{HorP}$. The last intermediate layer (one layer before the output layer) must be constructed such that it exhibits a scalar function value (i.e., output size is 1). This is to obtain the directional derivative for the output of the intermediate layer in the output layer.

Output Layer We construct a horizontal lift $\text{HorL} : (\mathbb{R}, \text{St}(k, D)) \rightarrow T_{\mathbf{Y}}^h \text{St}(k, D)$ as an output layer. In the horizontal lift layer HorL , a horizontal vector on the horizontal space $T_{\mathbf{Y}}^h \text{St}(k, D)$ with the origin \mathbf{Y} is obtained by directional derivative of the intermediate layer v_{out} with \mathbf{Y} .

$$\text{HorL}(v_{\text{out}}, \mathbf{Y}) = P_{\mathbf{Y}}^h(\text{autograd}(v_{\text{out}}, \mathbf{Y})) \text{ s.t. } P_{\mathbf{Y}}^h(\mathbf{Z}) = (\mathbf{I}_D - \mathbf{Y}\mathbf{Y}^\top) \mathbf{Z}, \quad (8)$$

where $\text{autograd}(v_{\text{out}}, \mathbf{Y})$ is automatic differentiation (Paszke et al. (2017)) of \mathbf{Y} with respect to v_{out} , and $P_{\mathbf{Y}}^h(\mathbf{Z})$ is the projection of \mathbf{Z} onto the horizontal space $T_{\mathbf{Y}}^h \text{St}(k, D)$ at \mathbf{Y} .

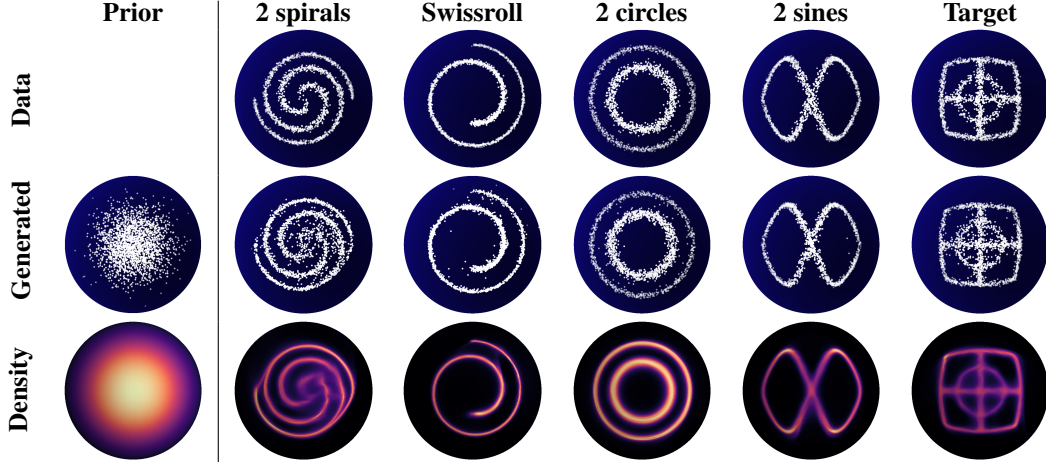


Figure 3: Generated samples and probability densities using the GrCNF trained on each of the five distributions. (top) Ground truth data, (middle) Generated data with the GrCNF when the leftmost column represents the prior distribution, and (bottom) densities obtained via training.

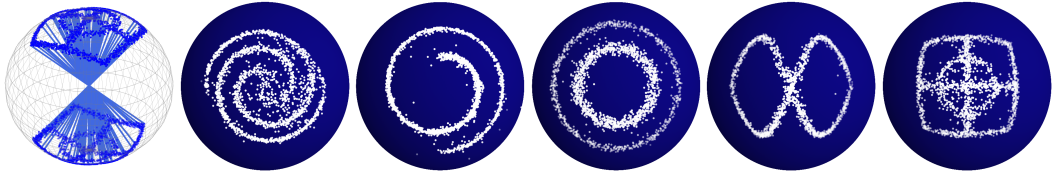


Figure 4: Results of the GrCNF transformation for the antipodal point of the prior in the middle panel of the Figure 3. The antipodal points are those that pass through the origin of the sphere and appear in the southern hemisphere (Leftmost). It is evident that the antipodal points are generated with exactly the same quality as in the Figure 3 for the un-trained antipodal points.

6 Experimental Results

In this section, we discuss the results of several experiments to evaluate the validity of GrCNF. Further details regarding each experimental condition, such as the architectures and hyperparameters used in training, can be found in Appendix C.3.

6.1 Generation and Density Estimation on Artificial Textures

We first train on five different $\text{Gr}(1, 3)$ (1-dimensional subspace in \mathbb{R}^3 , that is, a line through the origin) data to visualize the model and the trained dynamics. The five datasets³ were 2 spirals, Swissroll, 2 circles, 2 sines, and Target. We represented $\text{Gr}(1, 3)$ with a sphere of radius 1 centered at the origin by mapping a 1-dimensional subspace to two points on the sphere (a point on the sphere and its antipodal point) for visualization purposes.

Result The five types of probability densities transformed by GrCNF and the results of data generation are shown in Figure 3. The top, middle and the bottom rows in the figure shows the correct data, the generated data with GrCNF when the left-most column is the prior distribution, and the probability density on a $\text{Gr}(1, 3)$ obtained by training when the left-most column is the prior distribution, respectively. The probability density indicates that brighter the region, higher is the probability. The figure shows that GrCNF can generate high quality samples that are sufficiently accurate to the distribution of the correct data. To investigate whether the GrCNF learns the distribution on $\text{Gr}(1, 3)$, we generated antipodal points in Figure 3 with trained GrCNF used in Figure 3. As shown in Figure 4, GrCNF generated exactly the same high quality samples as the original for the untrained antipodal points. This experimental result implies that the proposed flow accurately learns the distribution on a $\text{Gr}(k, D)$ and that all the orthogonal transformed samples can be obtained with equal quality by only training with arbitrary representatives.

³We provide the code for the data distributions in Appendix C.3.1

Table 1: Negative log-likelihood comparison on the test partition of different methods for DW4 and LJ13 datasets for different amount of training samples averaged over 3 runs.

# of Samples	DW4				LJ13			
	10^2	10^3	10^4	10^5	10	10^2	10^3	10^4
GNF	-2.30	-7.04	-7.19	-7.93	6.77	-0.76	-4.26	-12.43
GNF-att	-2.02	-4.13	-5.25	-6.74	6.91	1.40	-6.81	-12.05
GNF-att-aug	-3.11	-4.04	-6.51	-9.42	2.95	-6.11	-13.94	-15.74
Simple dynamics	-1.22	-1.28	-1.36	-1.39	-1.10	-3.87	-3.72	-3.59
E-NF	-0.54	-9.89	-12.15	-15.29	-12.86	-15.75	-31.51	-32.83
GrCNF	-12.53	-13.74	-14.09	-16.07	-23.64	-44.24	-58.02	-58.71

6.2 Comparison with Conventional Methods on DW4 and LJ13

This study performed comparative experiments using DW4 and LJ13, the two systems presented by Köhler et al. (2020). These data sets were generated synthetically by sampling from their respective energy functions using Markov chain Monte Carlo (MCMC) methods. Both energy functions (DW4 and LJ13) are ideal for analyzing the advantages of various methods when they exist on data that are equivariant for rotation and reflection, respectively. We used the datasets generated by MCMC that have been used in Köhler et al. (2020). The orthonormalized data \mathbf{Y} was used for this study by applying Gram-Schmidt’s orthogonalization to each column of \mathbf{P} such that the D -dimensional data was a matrix with k orthonormal basis vectors (DW4: $D = 4, k = 2$, LJ13: $D = 13, k = 3$).

To match the experiment conducted in Garcia Satorras et al. (2021), 1,000 validation and testing samples each were used for both datasets. For DW4 and LJ13, different numbers of training samples, $\{10^2, 10^3, 10^4, 10^5\}$ and $\{10, 10^2, 10^3, 10^4\}$, respectively, were selected and their performances for each amount of data were examined. The proposed approach was compared to the state-of-the-art E(n) equivariant flow (E-NF) presented by Garcia Satorras et al. (2021) and Simple dynamics by Köhler et al. (2020). In addition, comparisons with graph normalizing flow (GNF), GNF with attention (GNF-att), and GNF with attention and data augmentation (GNF-att-aug) (data augmentation by rotation), which are non-equivariant variants of E-NF, were performed. All reported values were averages of cross-validations (three runs). Otherwise, the network structures of all these conventional methods were the same as in Garcia Satorras et al. (2021).

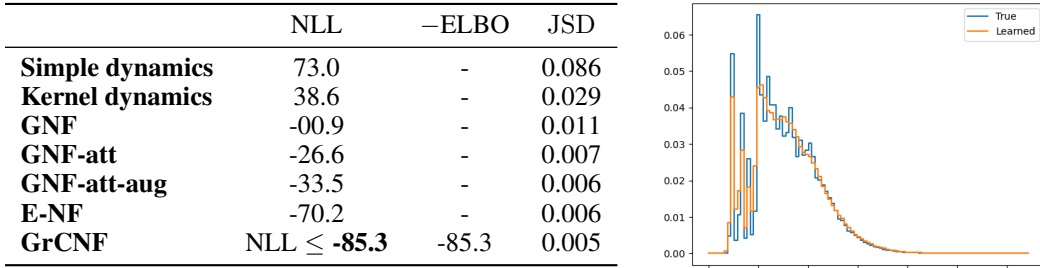
Result Table 1 shows the results of the cross-validated experiments (Negative log-likelihood; NLL) for the test samples. The proposed GrCNF outperformed both the conventional non-equivariant models (GNF, GNF-att and GNF-att-aug) and conventional equivariant models (Simple dynamics, E-NF) in all data domains.

6.3 Comparison with Conventional Methods on QM9 Positional

A comparative experiment was performed using QM9 Positional, a subset of the QM9 molecular dataset that considers only positional information. The purpose of this experiment was to evaluate the feasibility of generating a practical point cloud. The QM9 Positional comprises only molecules with 19 atoms/nodes, and each node has a 3-dimensional position vector associated with it. However, the likelihood of the molecules must be invariant to translation and rotation in 3-dimensional space; thus, the proposed model is suitable for this type of data. The dataset consists of 13,831, 2501, and 1813 training, validation, and testing samples each. In this experiment, we used evaluation metrics based on the NLL and Jensen-Shannon divergence (JSD) (Lin (1991)), based on the experiments conducted in Garcia Satorras et al. (2021). The JSD calculates the distance between the normalized histograms that are generated from the model and obtained from the training set, by creating a histogram of the relative distances between all the node pairs in each molecule.

GrCNF handles subspace data. Therefore, orthonormalized data \mathbf{Y} was used only in the proposed GrCNF, as in $\mathbf{P}\mathbf{P}^\top \simeq \mathbf{Y}\Lambda\mathbf{Y}^\top$ s.t. Λ is diagonal (Huang et al. (2015)), such that the k -dimensional point cloud data \mathbf{P} of N points $N \times k$ matrix is a matrix with k orthonormal basis vectors. However, a complete point cloud generating task, such as QM9 Positional, must also store a scale parameter $\sqrt{\Lambda}$ such that $\mathbf{P} = \mathbf{Y}\sqrt{\Lambda}$. Therefore, GrCNF incorporates an additional architecture to estimate $\sqrt{\Lambda}$. In addition, the proposed GrCNF encounters difficulties in computing the NLL in distribution

Table 2: Results for the QM9 Positional dataset. (Left) Negative log-likelihood, $-\text{ELBO}$ and JSD for the QM9 Positional dataset on the test data, and (Right) normalized histogram of relative distances between atoms for QM9 Positional and generated samples with GrCNF.



$p_\psi(\mathbf{P})$ of \mathbf{P} ; thus, a new loss function is required to address this. This study maximized the evidence lower bound (ELBO), the lower bound of the log-likelihood $\log p_\psi(\mathbf{P})$, using a variational inference framework. This is equal to the minimization of $-\text{ELBO}(\mathbf{P})$. Further details regarding ELBO can be found in Appendix C.2.2.

We compared our GrCNF with the GNF, GNF-att, GNF-att-aug, Simple dynamics, Kernel dynamics, and E-NF methods. The network structure and experimental conditions for all of these conventional methods were the same as in Garcia Satorras et al. (2021). Further, in all experiments, the training was done for 160 epochs. The JSD values were the average of the last 10 epochs for all models.

Result Table 2 (Left) shows the NLL, and JSD cross-validated against the test data. Although the proposed GrCNF cannot directly compute the NLL in this problem setting, it can still be concluded that GrCNF outperformed all other algorithms because the relation $\text{NLL} \leq -\text{ELBO}$ is true in general. With respect to JSD, GrCNF achieved the best performance. Table 2 (Right) shows the normalized histograms of the QM9 Positional molecular data and the generated data by GrCNF, in relation to the JSD of GrCNF, respectively. This shows that the histograms of the molecules generated by GrCNF are close to the histograms of the data set; that is, GrCNF can generate realistic molecules.

7 Conclusion

This study proposed the concept of CNF on a Grassmann manifold (GrCNF). This is a generative model that handles subspace data; that is, it is a continuous-time normalizing flow that considers the equivariance on the Stiefel manifold. Through suitable experiments, the ability of the proposed GrCNF to generate qualitatively in 1-dimensional subspace datasets in \mathbb{R}^3 was confirmed. Further, it was demonstrated that GrCNF significantly outperformed existing normalizing flows methods in terms of log-likelihood or ELBO in DW4, LJ13, and QM9 Positional.

Further considerations Our work is concerned with accurately modelling data topology, so we do not expect there to be any negative consequence in our application field. The proposed theory and implementation are valid in a remarkably general setting, although there are still certain limitations that can be addressed in future works: **1.** The CNF introduces the adjoint method to reduce memory utilization; however, it was not used in this study because it must be executed on $\text{Gr}(k, D)$. Lou et al. (2020) proposed a CNF on a manifold, and such a method must be introduced to GrCNF to handle larger and higher dimensional data sets in the future. **2.** The proposed method requires a calculation of inverse matrix and projection operation onto the manifold at each ODE step (Appendix C.1), which is computationally expensive.

References

P.-A. Absil, R. Mahony, and R. Sepulchre. *Optimization Algorithms on Matrix Manifolds*. Princeton University Press, 2008.

Taleb Alashkar, Boulbaba Ben Amor, Mohamed Daoudi, and Stefano Berretti. A grassmann framework for 4d facial shape analysis. *Pattern Recognition*, 57:21–30, 2016. ISSN 0031-3203.

E. Begelfor and M. Werman. Affine invariance revisited. In *2006 IEEE Computer Society Conference on Computer Vision and Pattern Recognition (CVPR'06)*, volume 2, pp. 2087–2094, 2006.

Camille Bilodeau, Wengong Jin, Tommi Jaakkola, Regina Barzilay, and Klavs F. Jensen. Generative models for molecular discovery: Recent advances and challenges. *WIREs Computational Molecular Science*, pp. e1608, 2022.

Denis Boyda, Gurtej Kanwar, Sébastien Racanière, Danilo Jimenez Rezende, Michael S. Albergo, Kyle Cranmer, Daniel C. Hackett, and Phiala E. Shanahan. Sampling using $su(n)$ gauge equivariant flows. *Phys. Rev. D*, 103(7):074504, 2021a.

Denis Boyda, Gurtej Kanwar, Sébastien Racanière, Danilo Jimenez Rezende, Michael S. Albergo, Kyle Cranmer, Daniel C. Hackett, and Phiala E. Shanahan. Sampling using $su(n)$ gauge equivariant flows. *Physical Review D*, 103(7), 2021b.

Elena Celledoni and Brynjulf Owren. A class of intrinsic schemes for orthogonal integration. *SIAM Journal on Numerical Analysis*, 40(6):2069–2084, 2002.

Ricky T. Q. Chen, Yulia Rubanova, Jesse Bettencourt, and David K Duvenaud. Neural ordinary differential equations. In *Advances in Neural Information Processing Systems*, volume 31, pp. 6571–6583, 2018.

Yasuko Chikuse. *Statistics on Special Manifolds. Lecture Notes in Statistics*, volume 174. Springer, 01 2003.

Taco Cohen, Maurice Weiler, Berkay Kicanaoglu, and Max Welling. Gauge equivariant convolutional networks and the icosahedral CNN. In *Proceedings of the 36th International Conference on Machine Learning*, volume 97, pp. 1321–1330, 2019a.

Taco S. Cohen and Max Welling. Group equivariant convolutional networks. In *Proceedings of The 33rd International Conference on Machine Learning*, volume 48, pp. 2990–2999, 2016.

Taco S. Cohen and Max Welling. Steerable cnns. In *International Conference on Learning Representations*, 2017.

Taco S. Cohen, Mario Geiger, Jonas Köhler, and Max Welling. Spherical cnns. In *International Conference on Learning Representations*, 2018.

Taco S. Cohen, Mario Geiger, and Maurice Weiler. A general theory of equivariant cnns on homogeneous spaces. In *Advances in Neural Information Processing Systems*, volume 32, 2019b.

R. J. Dormand and J. P. Prince. A family of embedded Runge-Kutta formulae. *Journal of Computational and Applied Mathematics*, pp. 19–26, 1980.

Olga Doronina, Zachary Grey, and Andrew Glaws. Grassmannian shape representations for aerodynamic applications. In *AAAI 2022 Workshop on AI for Design and Manufacturing (ADAM)*, 2022.

Alan Edelman, Tomás A. Arias, and Steven T. Smith. The geometry of algorithms with orthogonality constraints. *SIAM Journal on Matrix Analysis and Applications*, 20(2):303–353, 1998.

Lawrence Craig Evans and Gariepy Ronald. *Measure Theory and Fine Properties of Functions, Revised Edition (1st ed.)*. CRC Press, Revised Edition, 2015.

Yong Fan, Yong Liu, Hong Wu, Yihui Hao, Haihong Liu, Zhenning Liu, and Tianzi Jiang. Discriminant analysis of functional connectivity patterns on grassmann manifold. *NeuroImage*, 56(4):2058–2067, 2011.

Marc Finzi, Samuel Stanton, Pavel Izmailov, and Andrew Gordon Wilson. Generalizing convolutional neural networks for equivariance to lie groups on arbitrary continuous data. In *Proceedings of the 37th International Conference on Machine Learning*, volume 119, pp. 3165–3176, 2020.

Simone Fiori, Tetsuya Kaneko, and Toshihisa Tanaka. Tangent-bundle maps on the grassmann manifold: Application to empirical arithmetic averaging. *IEEE Transactions on Signal Processing*, 63(1):155–168, 2015.

Victor Garcia Satorras, Emiel Hoogeboom, Fabian Fuchs, Ingmar Posner, and Max Welling. $E(n)$ equivariant normalizing flows. In *Advances in Neural Information Processing Systems*, volume 34, pp. 4181–4192, 2021.

Bernardo B. Gatto, Juan G. Colonna, Eulanda M. dos Santos, and Eduardo F. Nakamura. Mutual singular spectrum analysis for bioacoustics classification. In *2017 IEEE 27th International Workshop on Machine Learning for Signal Processing (MLSP)*, pp. 1–6, 2017.

Evan S. Gawlik and M. Leok. High-order retractions on matrix manifolds using projected polynomials. *SIAM J. Matrix Anal. Appl.*, 39:801–828, 2018a.

Evan S. Gawlik and Melvin Leok. High-order retractions on matrix manifolds using projected polynomials. *SIAM Journal on Matrix Analysis and Applications*, 39(2):801–828, 2018b.

Mathieu Germain, Karol Gregor, Iain Murray, and Hugo Larochelle. Made: Masked autoencoder for distribution estimation. In *Proceedings of the 32nd International Conference on Machine Learning*, volume 37 of *Proceedings of Machine Learning Research*, pp. 881–889. PMLR, 2015.

Simon Graham, David B. A. Epstein, and Nasir M. Rajpoot. Dense steerable filter cnns for exploiting rotational symmetry in histology images. *IEEE Trans. Medical Imaging*, 39(12):4124–4136, 2020.

Will Grathwohl, Ricky T. Q. Chen, Jesse Bettencourt, Ilya Sutskever, and David Duvenaud. Ffjord: Free-form continuous dynamics for scalable reversible generative models. *International Conference on Learning Representations*, 2019.

Pim De Haan, Maurice Weiler, Taco Cohen, and Max Welling. Gauge equivariant mesh cnns: Anisotropic convolutions on geometric graphs. In *International Conference on Learning Representations*, 2021.

Ernst Hairer. *Geometric Numerical Integration : Structure-Preserving Algorithms for Ordinary Differential Equations*. Springer, 2nd ed. edition, 2006.

Yuval Haitman, Joseph M. Francos, and Louis L. Scharf. Grassmannian dimensionality reduction for optimized universal manifold embedding representation of 3d point clouds. In *2021 IEEE/CVF International Conference on Computer Vision Workshops (ICCVW)*, pp. 4196–4204, 2021.

Jihun Ham and Daniel D. Lee. Grassmann discriminant analysis: a unifying view on subspace-based learning. In *ICML '08*, 2008.

Mehrtash T. Harandi, Conrad Sanderson, Sareh Shirazi, and Brian C. Lovell. Graph embedding discriminant analysis on grassmannian manifolds for improved image set matching. In *CVPR 2011*, 2011.

Yi Hong, Xiao Yang, Roland Kwitt, Martin Styner, and Marc Niethammer. Regression uncertainty on the grassmannian. In *Proceedings of the 20th International Conference on Artificial Intelligence and Statistics*, volume 54 of *Proceedings of Machine Learning Research*, pp. 785–793, 2017.

Zhiwu Huang, Ruijing Wang, Shiguang Shan, and Xilin Chen. Projection metric learning on grassmann manifold with application to video based face recognition. In *2015 IEEE Conference on Computer Vision and Pattern Recognition (CVPR)*, pp. 140–149, 2015.

Zhiwu Huang, Jiqing Wu, and Luc Van Gool. Building deep networks on grassmann manifolds. In *Proceedings of the Thirty-Second AAAI Conference on Artificial Intelligence (AAAI-18)*, pp. 3279–3286, 2018.

Sergey Ioffe and Christian Szegedy. Batch normalization: Accelerating deep network training by reducing internal covariate shift. In *Proceedings of the 32nd International Conference on Machine Learning*, volume 37 of *Proceedings of Machine Learning Research*, pp. 448–456. PMLR, 2015.

Arieh Iserles, Hans Z. Munthe-Kaas, Syvert P. Nørsett, and Antonella Zanna. Lie-group methods. *Acta Numerica*, 9:215–365, 2000.

Isay Katsman, Aaron Lou, Derek Lim, Qingxuan Jiang, Ser Nam Lim, and Christopher M De Sa. Equivariant manifold flows. In *Advances in Neural Information Processing Systems*, volume 34, pp. 10600–10612, 2021.

Hyeyoung Kim, Hyeyoung Lee, Woo Hyun Kang, Joun Yeop Lee, and Nam Soo Kim. Softflow: Probabilistic framework for normalizing flow on manifolds. In *Advances in Neural Information Processing Systems*, volume 33, pp. 16388–16397. Curran Associates, Inc., 2020.

Diederik P. Kingma and Max Welling. Auto-encoding variational bayes. In *2nd International Conference on Learning Representations, ICLR 2014, Banff, AB, Canada, April 14-16, 2014, Conference Track Proceedings*, 2014.

Jonas Köhler, Leon Klein, and Frank Noe. Equivariant flows: Exact likelihood generative learning for symmetric densities. In *Proceedings of the 37th International Conference on Machine Learning*, volume 119, pp. 5361–5370, 2020.

Risi Kondor and Shubhendu Trivedi. On the generalization of equivariance and convolution in neural networks to the action of compact groups. In *Proceedings of the 35th International Conference on Machine Learning*, volume 80, pp. 2747–2755, 2018.

J.M. Lee. *Introduction to Smooth Manifolds*. Graduate Texts in Mathematics. Springer, 2003.

J. Lin. Divergence measures based on the shannon entropy. *IEEE Transactions on Information Theory*, 37(1):145–151, 1991.

Aaron Lou, Derek Lim, Isay Katsman, Leo Huang, Qingxuan Jiang, Ser-Nam Lim, and Christopher De Sa. Neural manifold ordinary differential equations. In *Proceedings of the 34th International Conference on Neural Information Processing Systems*, 2020.

Yui Man Lui. Advances in matrix manifolds for computer vision. *Image Vision Comput.*, 30(6–7): 380–388, 2012.

J.R. Magnus and H. Neudecker. *Matrix Differential Calculus with Applications in Statistics and Econometrics*. Wiley Series in Probability and Statistics. Wiley, 2019.

Arak M. Mathai, Serge B. Provost, and Hans J. Haubold. The matrix-variate gaussian distribution. In *Multivariate Statistical Analysis in the Real and Complex Domains*, pp. 217–288. Springer International Publishing, 2022.

Emile Mathieu and Maximilian Nickel. Riemannian continuous normalizing flows. In *Proceedings of the 34th International Conference on Neural Information Processing Systems*, 2020.

Cleve Moler and Charles Van Loan. Nineteen dubious ways to compute the exponential of a matrix, twenty-five years later. *SIAM Review*, 45(1):3–49, 2003.

Hans Munthe-Kaas. High order runge-kutta methods on manifolds. *Applied Numerical Mathematics*, 29(1):115–127, 1999. Proceedings of the NSF/CBMS Regional Conference on Numerical Analysis of Hamiltonian Differential Equations.

Aaron Van Oord, Nal Kalchbrenner, and Koray Kavukcuoglu. Pixel recurrent neural networks. In *Proceedings of The 33rd International Conference on Machine Learning*, volume 48 of *Proceedings of Machine Learning Research*, pp. 1747–1756. PMLR, 2016.

Adam Paszke, Sam Gross, Soumith Chintala, Gregory Chanan, Edward Yang, Zachary DeVito, Zeming Lin, Alban Desmaison, Luca Antiga, and Adam Lerer. Automatic differentiation in pytorch. In *NIPS 2017 Workshop on Autodiff*, 2017.

Adam Paszke, Sam Gross, Francisco Massa, Adam Lerer, James Bradbury, Gregory Chanan, Trevor Killeen, Zeming Lin, Natalia Gimelshein, Luca Antiga, Alban Desmaison, Andreas Kopf, Edward Yang, Zachary DeVito, Martin Raison, Alykhan Tejani, Sasank Chilamkurthy, Benoit Steiner, Lu Fang, Junjie Bai, and Soumith Chintala. Pytorch: An imperative style, high-performance deep learning library. In *Advances in Neural Information Processing Systems*, volume 32, 2019.

Omri Puny, Matan Atzmon, Edward J. Smith, Ishan Misra, Aditya Grover, Heli Ben-Hamu, and Yaron Lipman. Frame averaging for invariant and equivariant network design. In *International Conference on Learning Representations*, 2022.

Prajit Ramachandran, Barret Zoph, and Quoc V. Le. Searching for activation functions. *CoRR*, abs/1710.05941, 2017.

Danilo Rezende and Shakir Mohamed. Variational inference with normalizing flows. In *Proceedings of the 32nd International Conference on Machine Learning*, volume 37, pp. 1530–1538, 2015.

Danilo Jimenez Rezende, Sébastien Racanière, Irina Higgins, and Peter Toth. Equivariant hamiltonian flows, 2019.

Benjamin Sanchez-Lengeling and Alán Aspuru-Guzik. Inverse molecular design using machine learning: Generative models for matter engineering. *Science*, 361(6400):360–365, 2018.

Hiroyuki Sato and Toshihiro Iwai. Optimization algorithms on the grassmann manifold with application to matrix eigenvalue problems. *Japan Journal of Industrial and Applied Mathematics*, 31: 355–400, 2014.

Víctor Garcia Satorras, Emiel Hoogeboom, and Max Welling. $e(n)$ equivariant graph neural networks. In *Proceedings of the 38th International Conference on Machine Learning*, volume 139 of *Proceedings of Machine Learning Research*, pp. 9323–9332. PMLR, 2021.

Erica K. Shimomoto, François Portet, and Kazuhiro Fukui. Text classification based on the word subspace representation. *Pattern Analysis and Applications*, 24(3):1075–1093, 2021.

Jascha Sohl-Dickstein, Eric Weiss, Niru Maheswaranathan, and Surya Ganguli. Deep unsupervised learning using nonequilibrium thermodynamics. In *Proceedings of the 32nd International Conference on Machine Learning*, volume 37 of *Proceedings of Machine Learning Research*, pp. 2256–2265. PMLR, 2015.

Lincon S. Souza, Bernardo B. Gatto, and Kazuhiro Fukui. Classification of bioacoustic signals with tangent singular spectrum analysis. In *ICASSP 2019 - 2019 IEEE International Conference on Acoustics, Speech and Signal Processing (ICASSP)*, pp. 351–355, 2019.

Lincon S. Souza, Bernardo B. Gatto, Jing-Hao Xue, and Kazuhiro Fukui. Enhanced grassmann discriminant analysis with randomized time warping for motion recognition. *Pattern Recognition*, 97:107028, 2020.

Lincon S. Souza, Naoya Sogi, Bernardo B. Gatto, Takumi Kobayashi, and Kazuhiro Fukui. Grassmannian learning mutual subspace method for image set recognition. *Neurocomputing*, 2022. ISSN 0925-2312.

A. Srivastava, S.H. Joshi, W. Mio, and Xiuwen Liu. Statistical shape analysis: clustering, learning, and testing. *IEEE Transactions on Pattern Analysis and Machine Intelligence*, 27(4):590–602, 2005.

Anuj Srivastava and Eric Klassen. Bayesian and geometric subspace tracking. *Advances in Applied Probability*, 36(1):43–56, 2004.

Pavan Turaga, Ashok Veeraraghavan, and Rama Chellappa. Statistical analysis on stiefel and grassmann manifolds with applications in computer vision. In *2008 IEEE Conference on Computer Vision and Pattern Recognition*, pp. 1–8, 2008.

Pavan Turaga, Ashok Veeraraghavan, Anuj Srivastava, and Rama Chellappa. Statistical computations on grassmann and stiefel manifolds for image and video-based recognition. *IEEE Transactions on Pattern Analysis and Machine Intelligence*, 33(11):2273–2286, 2011.

Maurice Weiler and Gabriele Cesa. General $e(2)$ -equivariant steerable cnns. In *Advances in Neural Information Processing Systems*, volume 32, 2019.

Zaiwen Wen and Wotao Yin. A feasible method for optimization with orthogonality constraints. *Mathematical Programming*, 142:397–434, 2013.

Zhu Xiaojing. A riemannian conjugate gradient method for optimization on the stiefel manifold. *Computational Optimization and Applications*, 67:73–110, 2017.

Ryoma Yataka and Kazuhiro Fukui. Three-dimensional object recognition via subspace representation on a grassmann manifold. In *Proceedings of the 6th International Conference on Pattern Recognition Applications and Methods*, pp. 208–216. SciTePress, 2017.

Ryoma Yataka, Kazuki Hirashima, Takafumi Matsuda, Tai Tanaka, Masato Gocho, and Masashi Shiraishi. Projection metric learning of updated-subspaces for radar target classification. In *2019 16th European Radar Conference (EuRAD)*, pp. 5–8, 2019.

Takao Yoshinuma, Hideitsu Hino, and Kazuhiro Fukui. Personal authentication based on 3d configuration of micro-feature points on facial surface. In *Image and Video Technology*, pp. 433–446. Springer International Publishing, 2016.

Xiaojing Zhu and Chun-Yan Duan. On matrix exponentials and their approximations related to optimization on the stiefel manifold. *Optimization Letters*, 13, 07 2019.

Xiaojing Zhu and Hiroyuki Sato. Cayley-transform-based gradient and conjugate gradient algorithms on grassmann manifolds. *Adv. Comput. Math.*, 47(4), 2021.

A Appendix Overview

First, we present the details of the various proofs of Section 4 in Appendix B. Next, in Appendix C, we describe the network layers for the building GrCNF, and the detailed model architectures, hyper-parameters, and implementation on the experiments. Finally, in Appendix D, we provide a summary of the fundamentals of a Grassmann manifold, which is the core concept of this study.

B Proofs

B.1 Proposition 1

First, we invoked the following two corollaries.

Corollary 1 (Diffeomorphism Invariance of Flows). *Let $F : \mathcal{M} \rightarrow \mathcal{N}$ be a diffeomorphism. If X is a smooth vector field over \mathcal{M} and θ is the flow of X , then the flow of $F_* X^4$ is $\eta_t = F \circ \theta_t \circ F^{-1}$, with domain $N_t = F(M_t)$ for each $t \in \mathbb{R}$.*

Proof. See Lee (2003, Corollary 9.14). \square

Corollary 2 (Homogeneity Property). *The horizontal lift $\bar{\xi}_Y^h$ at representative $Y \in \text{St}(k, D)$ relative to $\xi_{[Y]} \in T_{[Y]} \text{Gr}(k, D)$ satisfies the following homogeneity (equivariance) property with regard to $\forall Q \in \mathcal{O}(k)$.*

$$\bar{\xi}_{YQ}^h = \bar{\xi}_Y^h Q. \quad (9)$$

Proof. $\pi(Y) = \pi(YQ)$ is true for $\forall Y \in \text{St}(k, D), Q \in \mathcal{O}(k)$. Therefore, $\pi(Y) = (\pi \circ q)(Y)$ is true when defined as $q(Y) = YQ$. When the derivative $d\pi(\cdot)[\cdot]$ of both sides is applied to the horizontal lift $\bar{\xi}_Y^h$ of $\xi_{[Y]}$, the following is obtained:

$$d\pi(Y) \left[\bar{\xi}_Y^h \right] = d(\pi \circ q)(Y) \left[\bar{\xi}_Y^h \right] = d\pi(q(Y)) \left[dq(Y) \left[\bar{\xi}_Y^h \right] \right] = d\pi(YQ) \left[\bar{\xi}_Y^h Q \right]. \quad (10)$$

Moreover, from (100) which is definition of horizontal lift, the following equation is true.

$$\xi_{[Y]} = d\pi(Y) \left[\bar{\xi}_Y^h \right] = d\pi(YQ) \left[\bar{\xi}_{YQ}^h \right]. \quad (11)$$

Subsequently, we obtain the following equation.

$$\xi_{[Y]} = d\pi(YQ) \left[\bar{\xi}_{YQ}^h \right] = d\pi(YQ) \left[\bar{\xi}_Y^h Q \right]. \quad (12)$$

Finally, the uniqueness of the horizontal lift yields $\bar{\xi}_{YQ}^h = \bar{\xi}_Y^h Q$. \square

Proposition 1. *Let $\text{Gr}(k, D)$ be a Grassmann manifold, \mathbf{X} be any time-dependent vector field on $\text{Gr}(k, D)$, and $F_{\mathbf{X}, T}$ be a flow on a \mathbf{X} . Let $\bar{\mathbf{X}}$ be any time-dependent horizontal lift and $\bar{F}_{\bar{\mathbf{X}}, T}$ be a flow of $\bar{\mathbf{X}}$. $\bar{\mathbf{X}}$ is a vector field on $\text{St}(k, D)$ if and only if $\bar{F}_{\bar{\mathbf{X}}, T}$ is a flow on $\text{St}(k, D)$ and satisfies invariance condition $\bar{\mathbf{X}} \sim \bar{\mathbf{X}}'$ for all $\bar{F}_{\bar{\mathbf{X}}, T} \sim \bar{F}_{\bar{\mathbf{X}}', T}$. Therefore, \mathbf{X} is a vector field on $\text{Gr}(k, D)$ if and only if $F_{\mathbf{X}, T} := \left[\bar{F}_{\bar{\mathbf{X}}, T} \right]$ is a flow on $\text{Gr}(k, D)$, and vice versa.*

Proof. Flow $F_{\mathbf{X}, T}$ on $\text{Gr}(k, D) \Rightarrow$ Vector Field \mathbf{X} on $\text{Gr}(k, D)$. Let $\theta : \text{St}(k, D) \times \mathcal{O}(k) \rightarrow \text{St}(k, D), (Y, Q) \mapsto YQ$ be a map representing the right action of the orthogonal group. In addition, let $F_{\mathbf{X}, T}$ be a flow on $\text{Gr}(k, D)$ and $\bar{F}_{\bar{\mathbf{X}}, T}$ be a flow on $\text{St}(k, D)$. These satisfy $\bar{F}_{\bar{\mathbf{X}}, T} \sim$

⁴ F_* denotes the pushforward, that is, another notation for the differential of F .

$$\bar{F}_{\bar{\mathbf{X}},T}, \bar{F}_{\bar{\mathbf{X}}Q,T} \in F_{\mathbf{X},T}, \bar{F}_{\bar{\mathbf{X}},T} \in F_{\mathbf{X},T}.$$

$$\bar{\mathbf{X}}\left(t, \bar{F}_{\bar{\mathbf{X}}Q,t}(\mathbf{Y}Q)\right) = \bar{\mathbf{X}}\left(t, \bar{F}_{\bar{\mathbf{X}},t}(\mathbf{Y})Q\right) \quad (13)$$

$$= \frac{d}{dt} \left\{ \bar{F}_{\bar{\mathbf{X}},t}(\mathbf{Y})Q \right\} \quad (14)$$

$$= \frac{d}{dt} \left(\theta \circ \bar{F}_{\bar{\mathbf{X}},t} \right) (\mathbf{Y}) \quad (15)$$

$$= d(\theta)_{\mathbf{Y}} \left\{ \frac{d}{dt} \bar{F}_{\bar{\mathbf{X}},t}(\mathbf{Y}) \right\} \quad (16)$$

$$= d(\theta)_{\mathbf{Y}} \left\{ \bar{\mathbf{X}}\left(t, \bar{F}_{\bar{\mathbf{X}},t}(\mathbf{Y})\right) \right\} \quad (17)$$

$$= \bar{\mathbf{X}}\left(t, \bar{F}_{\bar{\mathbf{X}},t}(\mathbf{Y})\right)Q. \quad (18)$$

Thus, $\bar{\mathbf{X}} \sim \bar{\mathbf{X}}Q$ is true. Therefore, $\bar{\mathbf{X}}$ is the horizontal lift of the vector field \mathbf{X} on $\text{Gr}(k, D)$ and is unique for \mathbf{X} .

Flow $F_{\mathbf{X},T}$ on $\text{Gr}(k, D)$ \Leftarrow Vector Field \mathbf{X} on $\text{Gr}(k, D)$. Let $\theta : \text{St}(k, D) \times \mathcal{O}(k) \rightarrow \text{St}(k, D), (\mathbf{Y}, Q) \mapsto \mathbf{Y}Q$ be a map representing the right action of the orthogonal group. In addition, let $\bar{\mathbf{X}}$ be a vector field over a horizontal bundle $T^h \text{St}(k, D)$ on $\text{St}(k, D)$ and $\bar{F}_{\bar{\mathbf{X}},T}$ be its flow. From the Corollary 1,

$$\bar{F}_{\theta_* \circ \bar{\mathbf{X}},T} = \theta \circ \bar{F}_{\bar{\mathbf{X}},T} \circ \theta^{-1} \quad (19)$$

$$\bar{F}_{\theta_* \circ \bar{\mathbf{X}},T} \circ \theta = \theta \circ \bar{F}_{\bar{\mathbf{X}},T} \quad (20)$$

$$\bar{F}_{d(\theta)_{\mathbf{Y}} \bar{\mathbf{X}},T} \circ \theta = \theta \circ \bar{F}_{\bar{\mathbf{X}},T} \quad (21)$$

$$\bar{F}_{\bar{\mathbf{X}}Q,T}(\mathbf{Y}Q) = \bar{F}_{\bar{\mathbf{X}},T}(\mathbf{Y})Q. \quad (22)$$

Note that $d(\theta)_{\mathbf{Y}} \bar{\mathbf{X}} = \bar{\mathbf{X}}Q$ is derived from the Corollary 2 and (4) in Zhu & Sato (2021). This indicates that $\bar{F}_{\bar{\mathbf{X}},T} \sim \bar{F}_{\bar{\mathbf{X}}',T}$ is true for any $\bar{\mathbf{X}}, \bar{\mathbf{X}}' \in T^h \text{St}(k, D)$ that satisfies $\bar{\mathbf{X}} \sim \bar{\mathbf{X}}'$. Thus, a new flow can be defined as $F_{\mathbf{X},T} := [\bar{F}_{\bar{\mathbf{X}},T}]$. This is a flow on a $\text{Gr}(k, D)$. Because $\bar{\mathbf{X}}$ is a vector field in a horizontal bundle $T^h \text{St}(k, D)$ on $\text{St}(k, D)$, it is a horizontal lift of the vector field \mathbf{X} on $\text{Gr}(k, D)$ and is therefore unique for \mathbf{X} .

Based on this, it can be concluded that the subject is satisfied. \square

B.2 Proposition 2

Proposition 2. *Let $\text{Gr}(k, D)$ be a Grassmann manifold. Let p be the probability density on $\text{Gr}(k, D)$ and F be the flow on $\text{Gr}(k, D)$. Suppose \bar{p} is a density on $\text{St}(k, D)$ and \bar{F} is a flow on $\text{St}(k, D)$. Then, the distribution $\bar{p}_{\bar{F}}$ after transformations by \bar{F} is also a density on $\text{St}(k, D)$. Further, the invariance condition $\bar{p}_{\bar{F}} \sim \bar{p}_{\bar{F}'}$ is satisfied for all $\bar{F} \sim \bar{F}'$. Therefore, $p_F := [\bar{p}_{\bar{F}}]$ is a distribution on $\text{Gr}(k, D)$.*

Proof. Let $\theta : \text{St}(k, D) \times \mathcal{O}(k) \rightarrow \text{St}(k, D) : (\mathbf{Y}, \mathbf{Q}) \mapsto \mathbf{Y}\mathbf{Q}$ be a map representing the right action of the orthogonal group.

$$\bar{p}_F(\theta \circ \mathbf{Y}) = \bar{p}_F(\theta \circ \mathbf{Y}) \frac{|\det\{J_\theta(\mathbf{Y})\}|}{|\det\{J_\theta(\mathbf{Y})\}|} = \frac{\bar{p}_{\theta^{-1} \circ F}(\mathbf{Y})}{|\det\{J_\theta(\mathbf{Y})\}|} \quad (23)$$

$$= \bar{p}((F^{-1} \circ \theta)(\mathbf{Y})) \frac{|\det\{J_{F^{-1} \circ \theta}(\mathbf{Y})\}|}{|\det\{J_\theta(\mathbf{Y})\}|} \quad (24)$$

$$= (\bar{p} \circ F^{-1}) \circ \theta(\mathbf{Y}) \frac{|\det\{J_{\theta \circ F^{-1}}(\mathbf{Y})\}|}{|\det\{J_\theta(\mathbf{Y})\}|} \quad (25)$$

$$= \theta \circ (\bar{p} \circ F^{-1})(\mathbf{Y}) \frac{|\det\{J_\theta(F^{-1}(\mathbf{Y})) J_{F^{-1}}(\mathbf{Y})\}|}{|\det\{J_\theta(\mathbf{Y})\}|} \quad (26)$$

$$= \theta \circ (\bar{p} \circ F^{-1})(\mathbf{Y}) \frac{|\det\{J_\theta(F^{-1}(\mathbf{Y}))\}| |\det\{J_{F^{-1}}(\mathbf{Y})\}|}{|\det\{J_\theta(\mathbf{Y})\}|} \quad (27)$$

$$= \theta \circ \bar{p}(F^{-1})(\mathbf{Y}) |\det\{J_{F^{-1}}(\mathbf{Y})\}| \frac{|\det\{J_\theta(F^{-1}(\mathbf{Y}))\}|}{|\det\{J_\theta(\mathbf{Y})\}|} \quad (28)$$

$$= \theta \circ \bar{p}_F(\mathbf{Y}) \frac{|\det\{J_\theta(F^{-1}(\mathbf{Y}))\}|}{|\det\{J_\theta(\mathbf{Y})\}|} \quad (29)$$

$$= \theta \circ \bar{p}_F(\mathbf{Y}), \quad (30)$$

where $|\det\{J_\theta(\mathbf{X})\}| = 1$ is true because θ is the action of the orthogonal group. Therefore, as $\bar{p}_F(\theta \circ \mathbf{Y}) = \theta \circ \bar{p}_F(\mathbf{Y})$ is true, $\bar{p}_F \sim \bar{p}_F \mathbf{Q} \in p_F$ is true. Based on this, it can be concluded that the subject is satisfied. \square

B.3 Proposition 3

Proposition 3. *The distribution $p_{\text{Gr}(k, D)}$ on a Grassmann manifold $\text{Gr}(k, D)$ based on the matrix-variate Gaussian distribution \mathcal{MN} can be expressed as follows.*

$$p_{\text{Gr}(k, D)}([\mathbf{X}]; [\mathbf{M}], \mathbf{U}, \mathbf{V}) = V_{\text{Gr}(k, D)} \mathcal{MN}\left(\bar{\xi}_M^h; \mathbf{0}, \mathbf{U}, \mathbf{V}\right) \left| \det\left(\frac{d\bar{R}_M}{d\bar{\xi}_M^h}\right) \right|, \quad (31)$$

where \mathbf{M} is an orthonormal basis matrix denoting the mean of the distribution, \mathbf{U} is a positive definite matrix denoting the row directional variance, \mathbf{V} is a positive definite matrix denoting the column directional variance, and $\bar{\xi}_M^h$ is a random sample from \mathcal{MN} in an $k(D-k)$ -dimensional horizontal space $T_M^h \text{St}(k, D)$. $V_{\text{Gr}(k, D)}$ denotes the total volume of $\text{Gr}(k, D)$ defined by (115), \bar{R}_M denotes the horizontal retraction at \mathbf{M} , and $|\det(d\bar{R}_M/d\bar{\xi}_M^h)|$ denotes the Jacobian.

Proof. Let $p_{\text{Gr}}([\mathbf{X}])$ be a probability density function on a $\text{Gr}(k, D)$. From (103), let $(d\mathbf{X})$ be the invariant measure on $\text{Gr}(k, D)$ and $d\bar{\xi}_M^h$ be the Lebesgue measure on $T_M^h \text{St}(k, D)$. Subsequently, a change of variables was performed according to the following:

$$p_{\text{Gr}(k, D)}([\mathbf{X}]) (d\mathbf{X}) = p_{\text{Gr}(k, D)}\left(\left[\bar{R}_M\left(\bar{\xi}_M^h\right)\right]\right) d\bar{\xi}_M^h, \quad (32)$$

$$p_{\text{Gr}(k, D)}([\mathbf{X}]) = p_{\text{Gr}(k, D)}\left(\left[\bar{R}_M\left(\bar{\xi}_M^h\right)\right]\right) \left| \det\left(\frac{d\bar{\xi}_M^h}{d\bar{R}_M}\right) \right|, \quad (33)$$

$$p_{\text{Gr}(k, D)}([\mathbf{X}]) = p_{\text{Gr}(k, D)}\left(\left[\bar{R}_M\left(\bar{\xi}_M^h\right)\right]\right) \left| \det\left(\frac{d\bar{R}_M}{d\bar{\xi}_M^h}\right) \right|^{-1}. \quad (34)$$

Suppose $p_{\text{Gr}}([\mathbf{X}])$ is integrable with the probability measure $[d\mathbf{X}]$ on $\text{Gr}(k, D)$ defined by (116). Then, we obtain the following relation.

$$\int_{\text{Gr}(k, D)} p_{\text{Gr}(k, D)}([\mathbf{X}]) [d\mathbf{X}] \quad (35)$$

$$= \frac{1}{V_{\text{Gr}(k, D)}} \int_{\text{Gr}(k, D)} p_{\text{Gr}(k, D)}([\mathbf{X}]) (d\mathbf{X}) \quad (36)$$

$$= \frac{1}{V_{\text{Gr}(k, D)}} \int_{T_M^h \text{St}(k, D)} p_{\text{Gr}(k, D)} \left(\left[\bar{R}_M \left(\bar{\xi}_M^h \right) \right] \right) \left| \det \left(\frac{d\bar{R}_M}{d\bar{\xi}_M^h} \right) \right|^{-1} d\bar{\xi}_M^h. \quad (37)$$

In addition, we obtain the following equation based on $[d\mathbf{X}]$.

$$\int_{\text{Gr}(k, D)} p_{\text{Gr}(k, D)}([\mathbf{X}]) [d\mathbf{X}] = \int_{T_M^h \text{St}(k, D)} \mathcal{MN} \left(\bar{\xi}_M^h \right) d\bar{\xi}_M^h = 1, \quad (38)$$

where $\mathcal{MN} \left(\bar{\xi}_M^h \right)$ denotes the matrix-variate Gaussian distribution (Mathai et al. (2022)). Thus, the probability density function on $\text{Gr}(k, D)$ can be expressed as follows:

$$p_{\text{Gr}(k, D)} \left(\left[\bar{R}_M \left(\bar{\xi}_M^h \right) \right] \right) = V_{\text{Gr}(k, D)} \mathcal{MN} \left(\bar{\xi}_M^h \right) \left| \det \left(\frac{d\bar{R}_M}{d\bar{\xi}_M^h} \right) \right|. \quad (39)$$

The Jacobian can be represented as $\left| \det \left(\frac{d\bar{R}_M}{d\bar{\xi}_M^h} \right) \right| = \left| \det \left\{ (\nabla \bar{R}_M)^\top (\nabla \bar{R}_M) \right\} \right|^{\frac{1}{2}}$ from Evans & Ronald (2015). Further, $\nabla \bar{R}_M$ can be computed as follows. First, we define the horizontal retraction $\bar{R}_Y : T_Y^h \text{St}(k, D) \rightarrow \text{St}(k, D)$ based on the Cayley transform from Zhu & Sato (2021).

$$\mathbf{X} = \bar{R}_M \left(\bar{\xi}_M^h \right) = \mathbf{M} + \bar{\xi}_M^h - \left(\frac{1}{2} \mathbf{M} + \frac{1}{4} \bar{\xi}_M^h \right) \left(\mathbf{I}_k + \frac{1}{4} \bar{\xi}_M^h \top \bar{\xi}_M^h \right)^{-1} \bar{\xi}_M^h \top \bar{\xi}_M^h. \quad (40)$$

This is a fixed time ($t = 1$) version of (124). Next, for improved visibility in subsequent calculations, let $\mathbf{E} = \bar{\xi}_M^h$, $\mathbf{F} = \frac{1}{2} \mathbf{M} + \frac{1}{4} \mathbf{E}$, $\mathbf{G} = (\mathbf{I}_k + \frac{1}{4} \mathbf{H})^{-1}$, $\mathbf{H} = \mathbf{E}^\top \mathbf{E}$. In addition, let \mathbf{D} be defined as the operator for the derivative of a matrix by a matrix. Then, the derivative $\nabla \bar{R}_M = \mathbf{D} \mathbf{X}$ by \mathbf{E} is as follows:

$$\mathbf{D} \mathbf{X} = \mathbf{D} \mathbf{M} + \mathbf{D} \mathbf{E} - \mathbf{D} (\mathbf{F} \mathbf{G} \mathbf{H}). \quad (41)$$

Finally, each derivative can be calculated as follows:

$$\mathbf{D} \mathbf{M} = \mathbf{0}, \quad (42)$$

$$\mathbf{D} \mathbf{E} = \mathbf{I}_{Dk}, \quad (43)$$

$$\mathbf{D} (\mathbf{F} \mathbf{G} \mathbf{H}) = \mathbf{D} (\mathbf{F} (\mathbf{G} \mathbf{H})) \quad (44)$$

$$= \left\{ (\mathbf{G} \mathbf{H})^\top \otimes \mathbf{I}_D \right\} \mathbf{D} \mathbf{F} + (\mathbf{I}_k \otimes \mathbf{F}) \mathbf{D} (\mathbf{G} \mathbf{H}) \quad (45)$$

$$= \left\{ (\mathbf{G} \mathbf{H})^\top \otimes \mathbf{I}_D \right\} \mathbf{D} \mathbf{F} + (\mathbf{I}_k \otimes \mathbf{F}) \{ (\mathbf{H}^\top \otimes \mathbf{I}_k) \mathbf{D} \mathbf{G} + (\mathbf{I}_k \otimes \mathbf{G}) \mathbf{D} \mathbf{H} \} \quad (46)$$

$$= \left\{ (\mathbf{G} \mathbf{H})^\top \otimes \mathbf{I}_D \right\} \mathbf{D} \mathbf{F} + (\mathbf{I}_k \otimes \mathbf{F}) (\mathbf{H}^\top \otimes \mathbf{I}_k) \mathbf{D} \mathbf{G} + (\mathbf{I}_k \otimes \mathbf{F}) (\mathbf{I}_k \otimes \mathbf{G}) \mathbf{D} \mathbf{H} \quad (47)$$

$$= (\mathbf{G}^\top \mathbf{H}^\top \otimes \mathbf{I}_D) \mathbf{D} \mathbf{F} + (\mathbf{H}^\top \otimes \mathbf{F}) \mathbf{D} \mathbf{G} + (\mathbf{I}_k \otimes \mathbf{F} \mathbf{G}) \mathbf{D} \mathbf{H}, \quad (48)$$

$$\mathbf{D} \mathbf{F} = \mathbf{D} \left(\frac{1}{2} \mathbf{M} \right) + \mathbf{D} \left(\frac{1}{4} \mathbf{E} \right) = \frac{1}{4} \mathbf{D} \mathbf{E}, \quad (49)$$

$$\mathbf{D} \mathbf{G} = - (\mathbf{G}^\top \otimes \mathbf{G}) \mathbf{D} \mathbf{H}, \quad (50)$$

$$\mathbf{D} \mathbf{H} = (\mathbf{I}_{k^2} + \mathbf{K}_{k,k}) (\mathbf{I}_k \otimes \mathbf{E}^\top) \mathbf{D} \mathbf{E}, \quad (51)$$

where \otimes denotes the Kronecker product. $\mathbf{K}_{D,k}$ is a $Dk \times Dk$ matrix $\mathbf{K}_{D,k} = \sum_{i=1}^m \sum_{j=1}^n (\mathbf{L}_{i,j} \otimes \mathbf{L}_{i,j}^\top)$ referred to as the commutation matrix, which denotes the transposition operation of $D \times k$. Further, $\mathbf{L}_{i,j}$ is a $D \times k$ matrix whose (i, j) component is 1 whereas all other components are 0. \square

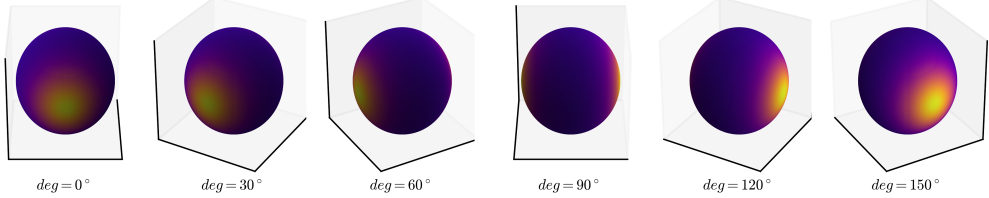


Figure 5: $p_{\text{Gr}(1,3)}([\mathbf{X}])$ with $\mathbf{M} = (1.0, 0.0, 0.0)^\top$, $\mathbf{U} = \sigma^2 \mathbf{I}_3$, $\mathbf{V} = \mathbf{I}_1$, $\sigma = 0.5$. Each sphere in the figure indicates $\text{Gr}(1, 3)$, with brighter spheres representing higher densities and conversely, darker spheres representing lower densities.

For details on the formulae for matrix derivatives used in this proof, please refer to Magnus & Neudecker (2019).

$p_{\text{Gr}(k, D)}([\mathbf{X}]) = p_{\text{Gr}(k, D)}([\mathbf{X}]; [\mathbf{M}], \mathbf{U}, \mathbf{V})$ is a probability distribution following mean $[\mathbf{M}]$ and matrix variance \mathbf{U}, \mathbf{V} . Using $\text{Gr}(1, 3)$ as an example, we qualitatively confirmed through visualization that $p_{\text{Gr}(1,3)}([\mathbf{X}])$ is density on $\text{Gr}(1, 3)$. $\text{Gr}(1, 3)$ is a 1-dimensional subspace on a 3-dimensional space; that is, a space whose elements are lines passing through the origin in 3-dimensional space. For the visualization, we expressed $\text{Gr}(1, 3)$ by mapping a 1-dimensional subspace to two points on the sphere (one point on the sphere and its antipodal point), using a sphere of radius 1 centered at the origin.

Figure 5 shows the density of $p_{\text{Gr}(1,3)}([\mathbf{X}])$ with $\mathbf{M} = (1.0, 0.0, 0.0)^\top$, $\mathbf{U} = \sigma^2 \mathbf{I}_3$, $\mathbf{V} = \mathbf{I}_1$, $\sigma = 0.5$. Each sphere in the figure indicates $\text{Gr}(1, 3)$, with brighter spheres representing higher densities and conversely, darker spheres representing lower densities. The leftmost figure shows \mathbf{M} as viewed from the front diagonally above, and the other figures present the views when the viewpoint is rotated clockwise around the z -axis by 30° to 150° with movement to the right. The leftmost figure shows that the density is highly spread around \mathbf{M} . Further, the other figures (particularly the rightmost one) show that the antipodal point $(-\mathbf{M} = (-1.0, 0.0, 0.0)^\top)$ is also densely spread out. This implies that by specifying only one \mathbf{M} as the representative of the equivalence class $[\mathbf{M}]$, the density around the other elements in the equivalence class $[\mathbf{M}]$ is as high as that around the representative. Thus, based on the above, we can confirm that $p_{\text{Gr}(k, D)}([\mathbf{X}])$ has a density of $\text{Gr}(1, 3)$.

C Experimental Details for Learning GrCNF

C.1 ODE Solver with Orthogonal Integration

We provide an ordinary differential equation (ODE) solver on $\text{Gr}(k, D)$. There are many studies of ODE solvers that work on a manifold \mathcal{M} (Munthe-Kaas (1999); Iserles et al. (2000); Hairer (2006)). Hairer (2006) proposed the simple projection method that projects onto the manifold at each step and the symmetric projection method suitable for long-time integration. However, these require that \mathcal{M} is a submanifold in Euclidean space, it cannot be applied on $\text{Gr}(k, D)$. On the other hand, Celledoni & Owren (2002) introduce an intrinsic ODE solver that works on a Stiefel manifold and does not assume an outer Euclidean space. The solver in Celledoni & Owren (2002) works on a Stiefel manifold, thus we need to reformulate it into a solver that works on $\text{Gr}(k, D)$, which is our problem setting. We introduce below a solver on $\text{Gr}(k, D)$ via ODE operating on the horizontal space $T_{\mathbf{Y}}^h \text{St}(k, D)$, based on results from Celledoni & Owren (2002) and Section 4. This approach is intrinsic in the sense that it does not depend on whether \mathcal{M} has been embedded in a bigger space with a corresponding extension of the vector field \mathbf{F} .

To begin with, let us consider an ODE given by means of a vector field \mathbf{X}_θ on a curve $\gamma(t) : [0, \infty) \rightarrow \text{St}(k, D)$ such that for each time t .

$$\frac{d\gamma(t)}{dt} = \mathbf{X}_\theta(t, \gamma(t)), \quad \gamma(0) = \mathbf{Y}, \quad (52)$$

where \mathbf{X}_θ is constructed by a neural network with parameter θ , as described in Section 5.3. Horizontal retraction $\bar{R}_{\mathbf{Y}}$ which is defined as (40) and is described in Appendix D.6, serves to define local coordinates of $\text{Gr}(k, D)$ in a neighborhood of the point $[\mathbf{Y}]$. We can thus represent the solution of ODE in the form:

$$\gamma(t) = \bar{R}_{\mathbf{Y}}(\epsilon(t)), \quad (53)$$

where $\epsilon : [0, \infty) \rightarrow T_{\mathbf{Y}}^h \text{St}(k, D)$ is the curve on $T_{\mathbf{Y}}^h \text{St}(k, D)$. By differentiating (53) with t , we obtain the following equation:

$$\frac{d\gamma(t)}{dt} = \frac{d}{dt} \bar{R}_{\mathbf{Y}}(\epsilon(t)) = \mathbf{X}_\theta(t, \gamma(t)). \quad (54)$$

Therefore, the ODE defined on $T_{\mathbf{Y}}^h \text{St}(k, D)$ is obtained:

$$\frac{d\text{Vec}(\epsilon(t))}{dt} = \left(\frac{d\bar{R}_{\mathbf{Y}}}{d\epsilon} \right)^{-1} \text{Vec}(\mathbf{X}_\theta(t, \bar{R}_{\mathbf{Y}}(\epsilon(t)))) , \quad (55)$$

where $d\bar{R}_{\mathbf{Y}}/d\epsilon$ can be calculated using (41) and Vec denotes the map of vertically concatenating matrices and converting them into a single vector. Because (55) is an ODE on $T_{\mathbf{Y}}^h \text{St}(k, D) \cong \mathbb{R}^{(D-k) \times k}$ from (Absil et al. (2008)), it can be solved using an ODE solver such as Runge-Kutta that operates on Euclidean space. In this paper, we use the Algorithm 5.1 in Celledoni & Owren (2002), and in each step, we first solve (55) using the Runge-Kutta of order 5 of Dormand-Prince-Shampine (Dormand & Prince (1980)), and then we obtain the solution of ODE (52) by applying the solution ϵ to (53).

C.2 Loss Functions

C.2.1 Loss Function for GrCNF

The total change in log-likelihood using GrCNF can be calculated using the following equation.

$$\log p_\theta(\mathbf{Y}(t_1)) = \log p_{\text{Gr}(k, D)}\left(F_{\mathbf{X}, t_1 \theta}^{-1}(\mathbf{Y}(t_1))\right) - \int_{t_0}^{t_1} \nabla \cdot \mathbf{X}_\theta(t, \mathbf{Y}(t)) dt. \quad (56)$$

In this study, we defined the loss function Loss for maximizing the log-likelihood as follows:

$$\text{Loss} = \text{NLL} = -\log p_\theta(\mathbf{Y}(t_1)), \quad (57)$$

where NLL denotes negative log-likelihood.

C.2.2 Loss Function based on Variational Inference

In the setting in Section 6.3, we used orthonormalized data \mathbf{Y} as in $\mathbf{P}\mathbf{P}^\top \simeq \mathbf{Y}\Lambda\mathbf{Y}^\top$, s.t. Λ is diagonal (Huang et al. (2015)), such that the k -dimensional point cloud data \mathbf{P} of N points $N \times k$ matrix is a matrix with k orthonormal basis vectors. Thus, generating a complete point cloud requires the estimation of the scale parameters $\sqrt{\Lambda}$ to be $\mathbf{P} = \mathbf{Y}\sqrt{\Lambda}$ and a loss function that incorporates this. In this study, we approximated by maximizing the evidence lower bound (ELBO), which is the lower bound of the overall log-likelihood $\log p_\psi(\mathbf{P})$ of $p_\psi(\mathbf{P})$, using a variational inference framework. The loss function is the variational energy – ELBO(\mathbf{P}) with negative ELBO.

$$\text{NLL} = -\log p_\psi(\mathbf{P}) \leq -\text{ELBO}(\mathbf{P}) = \text{Loss}. \quad (58)$$

ELBO(\mathbf{P}) can be decomposed as follows.

$$\text{ELBO}(\mathbf{P}) = \log p_\psi(\mathbf{P}) - D_{KL}(q_\phi(\mathbf{Y}|\mathbf{P})||p_\psi(\mathbf{Y}|\mathbf{P})) \quad (59)$$

$$= \mathbb{E}_{q_\phi(\mathbf{Y}|\mathbf{P})} [\log p_\psi(\mathbf{P}|\mathbf{Y})] - D_{KL}(q_\phi(\mathbf{Y}|\mathbf{P})||p_\theta(\mathbf{Y})), \quad (60)$$

where $q_\phi(\mathbf{Y}|\mathbf{P})$ is the inference model with parameter ϕ , $p_\psi(\mathbf{P}|\mathbf{Y})$ is the decoder model with parameter ψ , $p_\psi(\mathbf{Y}|\mathbf{P})$ is the posterior distribution with parameter ψ , and $p_\theta(\mathbf{Y})$ is the prior distribution with parameter θ . Further, $D_{KL}(q_\phi(\mathbf{Y}|\mathbf{P})||p_\theta(\mathbf{Y}))$ can be formulated using differential entropy as follows.

$$D_{KL}(q_\phi(\mathbf{Y}|\mathbf{P})||p_\theta(\mathbf{Y})) = -\mathbb{E}_{q_\phi(\mathbf{Y}|\mathbf{P})} [p_\theta(\mathbf{Y})] - H[q_\phi(\mathbf{Y}|\mathbf{P})]. \quad (61)$$

Thus, the final loss function is as follows.

$$\text{Loss} = -\text{ELBO}(\mathbf{P}) \quad (62)$$

$$= -\mathbb{E}_{q_\phi(\mathbf{Y}|\mathbf{P})} [\log p_\psi(\mathbf{P}|\mathbf{Y})] - \mathbb{E}_{q_\phi(\mathbf{Y}|\mathbf{P})} [p_\theta(\mathbf{Y})] - H[q_\phi(\mathbf{Y}|\mathbf{P})]. \quad (63)$$

Each term of the loss function can be calculated as follows.

Expectation of log-likelihood $\mathbb{E}_{q_\phi(\mathbf{Y}|\mathbf{P})} [\log p_\psi(\mathbf{P}|\mathbf{Y})]$ is the reconstruction log-likelihood of \mathbf{P} . The expectation is estimated by Monte Carlo sampling.

Differential entropy In the decomposition of a point cloud \mathbf{P} , there exists arbitrariness in the choice of \mathbf{Y} and Λ , as in $\mathbf{P}\mathbf{P}^\top \simeq \mathbf{Y}\Lambda\mathbf{Y}^\top$. In this study, we assumed that the diagonal components of Λ are in descending order, and we restricted the decomposition arbitrariness to be an action $\mathbf{Q} \in \mathcal{O}(k)$. If we suppose that the action \mathbf{Q} follows a uniform distribution when $\mathbf{Y} = \mathbf{X}\mathbf{Q}$ holds, then \mathbf{Y} also follows a uniform distribution in the k -dimensional subspace $\text{span}(\mathbf{Y})$. Although this is a uniform distribution on $\text{St}(k, k)$, we can consider a uniform distribution on $\mathcal{O}(k)$ because $\text{St}(k, k) = \mathcal{O}(k)$. The probability density function of \mathbf{Q} is represented by $U_{\mathcal{O}(k)}(\mathbf{Q})$ in (113). Therefore, the differential entropy of the decoder model can be calculated as follows.

$$H[q_\phi(\mathbf{Y}|\mathbf{P})] = \mathbb{E}[-\log q_\phi(\mathbf{Y}|\mathbf{P})] \quad (64)$$

$$= -\int_{\mathcal{O}(k)} U_{\mathcal{O}(k)}(\mathbf{Q}) \log U_{\mathcal{O}(k)}(\mathbf{Q}) [d\mathbf{Q}] \quad (65)$$

$$= -\int_{\mathcal{O}(k)} \frac{1}{V_{\mathcal{O}(k)}} \log \frac{1}{V_{\mathcal{O}(k)}} [d\mathbf{Q}] \quad (66)$$

$$= \frac{\log V_{\mathcal{O}(k)}}{V_{\mathcal{O}(k)}} \int_{\mathcal{O}(k)} [d\mathbf{Q}] \quad (67)$$

$$= \frac{\log V_{\mathcal{O}(k)}}{V_{\mathcal{O}(k)}}. \quad (68)$$

Expectation of prior distribution We used (56) for the prior distribution $p_\theta(\mathbf{Y})$. Further, re-parameterization was used to enable differentiable Monte Carlo estimation of expectations.

$$\mathbb{E}_{q_\phi(\mathbf{Y}|\mathbf{P})} [p_\theta(\mathbf{Y})] = \frac{1}{L} \sum_{l=1}^L p_\theta(\mathbf{X}\mathbf{Q}_l) \text{ s.t. } \mathbf{X} \sim \mathbf{Y}, \mathbf{Q}_l \in \mathcal{O}(k), \quad (69)$$

where it was assumed that \mathbf{Q} is sampled from a uniform distribution, which follows Haar measure on $\mathcal{O}(k)$. L is set $L = 1$.

Table 3: Network architectures for each experiment; (left) for the Simple Texture dataset, (middle) for the DW4 dataset, (right) for the LJ13 dataset.

GrCNF for Textures		
Layer	Out Size	Norm./Act.
Input	3×1	-
HorP	3×1	-/Tanh
Vec	3	-/-
TW	64	-/Tanh
TW	64	-/Tanh
TW	1	-/Tanh
HorL	3×1	-

GrCNF for DW4			GrCNF for LJ13		
Layer	Out Size	Norm./Act.	Layer	Out Size	Norm./Act.
Input	4×2	-	Input	13×3	-
HorP	4×2	-/Tanh	HorP	13×3	-/Tanh
Vec	8	-/-	Vec	39	-/-
TW	64	-/Tanh	TW	32	-/Tanh
TW	64	-/Tanh	TW	32	-/Tanh
TW	64	-/Tanh	TW	32	-/Tanh
TW	1	-/Tanh	TW	1	-/Tanh
HorL	4×2	-	HorL	13×3	-

C.3 Implementation Details and Experimental setting

The following sections present more details about the network architectures, training hyperparameters, and experimental conditions for each of the experiments in Section 6.

C.3.1 Artificial Textures

Network Architecture The vector field was constructed with the specific input, intermediate, and output layers described in Section 5.3. The GrCNF architecture is shown on top in Table 3. Layers are denoted as Layer in the table, and were processed from top to bottom. Norm. and Act. denote the normalization and activation functions to be applied immediately after the Layer, and the Norm. and Act. were applied in that order. Further, Out Size denotes the output size after Act. Vec denotes the map of vertically concatenating matrices and converting them into a single vector. Moreover, only row Input denotes the size of the input data, not the input layer (HorP). (57) was used for the loss function.

Hyper-parameters The mean \mathbf{M} and covariances \mathbf{U} and \mathbf{V} in the prior distribution on the Grassmann manifold were set to $\mathbf{M} = (1.0, 0.0, 0.0)^\top$, $\mathbf{U} = \sigma^2 \mathbf{I}_3$, and $\mathbf{V} = \mathbf{I}_1$, $\sigma = 0.3$, respectively. Other hyperparameters used during the training of GrCNF are shown in Table 4.

Implementation We used PyTorch (Paszke et al. (2019)) to implement the model and run the experiments. The CNF is based on the implementation⁵ in Chen et al. (2018) and the framework of the RCNF Mathieu & Nickel (2020). Thus, the ODE was solved using the explicit and adaptive Runge–Kutta method (Dormand & Prince (1980)) of order 5, and worked by projecting each step onto a manifold (Haider (2006)). The autograd in (8) was calculated with `torch.autograd.grad` (Paszke et al. (2017)) in PyTorch. The experimental hardware was built with an Intel Core i7-9700 CPU and a single NVIDIA GTX 1060 GPU with 6 GB of RAM.

⁵We used the authors’ implementation: <https://github.com/rtqichen/torchdiffeq.git>.

Table 4: List of hyperparameters used in various experiments. A “-” indicates that the hyperparameter is unused.

		Textures	DW4	LJ13	QM9
# of Data	Train	∞	$10^2/10^3/10^4/10^5$	$10/10^2/10^3/10^4$	13,831
	Validation	500	1000	1000	2,501
	Test	500	1000	1000	1,813
Optimizer	Name	Adam	Adam	Adam	Adam
	beta1	0.9	0.9	0.9	0.9
	beta2	0.999	0.999	0.999	0.999
	Weight Decay	-	1.0e-12	1.0e-12	1.0e-12
	Learning Rate	1.0e-3	1.0e-4	1.0e-4	5.0e-4
Schedule	Epoch	72000	1000/300/50/6	500/1000/300/50	160
	LR Step with 0.1	20000	-	-	-
	Batch Size	500	100	10/100/100/100	128
NeuralODE	Integration Time	Training	Training	Training	0.1
	atol	1.0e-5	1.0e-5	1.0e-5	1.0e-5
	rtol	1.0e-5	1.0e-5	1.0e-5	1.0e-5
	Adjoint	-	-	-	-

The code used in the experiment to generate the data distributions on $\text{Gr}(1, 3)$ is shown in Listing 1. This implementation of the data distributions is based on the codes in Kim et al. (2020) and Grathwohl et al. (2019)⁶.

Listing 1: Code for the data distributions.

```
import numpy as np

def get_data_batch(batch_size, dist):
    rng = np.random.RandomState()

    if dist == "2spirals":
        n = np.sqrt(rng.random(batch_size // 2, 1)) * 540 * (2 * np.pi) / 360
        d1x = -np.cos(n) * n + np.random.rand(batch_size // 2, 1) * 0.1
        d1y = np.sin(n) * n + np.random.rand(batch_size // 2, 1) * 0.1
        x = np.vstack((np.hstack((d1x, d1y)), np.hstack((-d1x, -d1y)))) / 3
        sample_2d = x + np.random.randn(*x.shape) * 0.1

    elif dist == "swissroll":
        data = sklearn.datasets.make_swiss_roll(n_samples=batch_size, noise=.3)[0]
        data = data.astype("float32")[:, [0, 2]]
        sample_2d = data / 5

    elif dist == "2circles":
        data = sklearn.datasets.make_circles(n_samples=batch_size, \
                                              factor=.5, noise=0.05)[0]
        data = data.astype("float32")
        sample_2d = data * 3

    elif dist == "2sines":
        x = (rng.rand(batch_size) - 0.5) * 2 * np.pi
        u = (rng.binomial(1, 0.5, batch_size) - 0.5) * 2
        y = u * np.sin(x) * 2.5
        x += np.random.randn(*x.shape) * 0.1
        y += np.random.randn(*y.shape) * 0.1
        sample_2d = np.stack((x, y), 1)

    elif dist == "target":
        shapes = np.random.randint(7, size=batch_size)
        mask = []
        for i in range(7):
            mask.append((shapes == i) * 1.)

    theta = np.linspace(0, 2 * np.pi, batch_size, endpoint=False)
```

⁶We used the authors’ implementations: <https://github.com/ANLGBOY/SoftFlow.git> and <https://github.com/rtqichen/ffjord.git>.

```

x = (mask[0] + mask[1] + mask[2]) * (rng.rand(batch_size) - 0.5) * 4 + \
    (-mask[3] + mask[4] * 0.0 + mask[5]) * 2 * np.ones(batch_size) + \
    mask[6] * np.cos(theta)
y = (mask[3] + mask[4] + mask[5]) * (rng.rand(batch_size) - 0.5) * 4 + \
    (-mask[0] + mask[1] * 0.0 + mask[2]) * 2 * np.ones(batch_size) + \
    mask[6] * np.sin(theta)
x += np.random.randn(*x.shape) * 0.1
y += np.random.randn(*y.shape) * 0.1
sample_2d = np.stack((x, y), 1)

norm = sample_2d / np.max(np.linalg.norm(sample_2d, axis=1))
sample_3d = np.concatenate((np.ones((batch_size, 1)), norm), axis=1)
return sample_3d / np.linalg.norm(sample_3d, axis=1)[:, np.newaxis]

```

C.3.2 DW4 and LJ13

Network Architecture As in Appendix C.3.1, the vector field was constructed with the specific input, intermediate, and output layers described in Section 5.3. The GrCNF architecture is shown on the bottom left and right in Table 3. The bottom left and right were used for experiments on the DW4 and LJ13 datasets, respectively. The views presented in the table is the same as in Appendix C.3.1. (57) was used for the loss function. In addition, for architectures in methods other than GrCNF, please refer to Garcia Satorras et al. (2021).

Hyperparameters The mean \mathbf{M} and covariances \mathbf{U} and \mathbf{V} in the prior distribution on the Grassmann manifold were set to $\mathbf{M} = \mathbf{I}_{4 \times 2}$, $\mathbf{U} = \sigma^2 \mathbf{I}_4$, and $\mathbf{V} = \sigma^2 \mathbf{I}_2$, $\sigma = 0.3$ for DW4 and $\mathbf{M} = \mathbf{I}_{13 \times 3}$, $\mathbf{U} = \sigma^2 \mathbf{I}_{13}$, and $\mathbf{V} = \sigma^2 \mathbf{I}_3$, $\sigma = 0.3$ for LJ13, respectively. Other hyperparameters used during the training of GrCNF are shown in Table 4. In addition, for the hyperparameters in methods other than GrCNF, please refer to Garcia Satorras et al. (2021).

Implementation The experimental hardware was built using a single NVIDIA Quadro RTX 8000 GPU with 48 GB of GDDR6 RAM. The other environments were the same as in Appendix C.3.1.

Full results In Tables 5 and 6, the same DW4 and LJ13 averaged results from Section 6.2 were reported; however, they included the standard deviations over the three runs.

C.3.3 QM9 Positional

Network Architecture On the QM9 Positional, we addressed the task of generating the molecular \mathbf{P} by estimating the scale parameter $\sqrt{\Lambda} = \text{diag} \left(\{\sqrt{\lambda_i}\}_{i=1}^3 \right)$, in addition to the generation of the orthonormal basis matrix \mathbf{Y} with GrCNF. Because the molecular generation task requires a specialized loss function based on variational inference, we used (58), as explained in Appendix C.2.2. We designed two networks to achieve this. The first is the same GrCNF architecture as in previous experiments, and the second is a scale estimator. Table 7 shows the architectures. The left side of the table shows the GrCNF architecture and the right side shows the scale estimator. The scale estimator estimated one scale parameter from each of the three orthonormal basis vectors $\mathbf{Y} = \{\mathbf{y}_i \in \mathbb{R}^{19}\}_{i=1}^3$, for a total of three parameters $\{\sqrt{\lambda_i} \in \mathbb{R}\}_{i=1}^3$. With the orthonormal orthogonal basis matrix \mathbf{Y} and the estimated scale parameter $\sqrt{\Lambda}$, we generated a point cloud $\mathbf{P} = \mathbf{Y} \sqrt{\Lambda}$. In this study, the overall architecture that generates \mathbf{P} is also named GrCNF.

Hyperparameters The mean \mathbf{M} and covariances \mathbf{U} and \mathbf{V} in the prior distribution on the Grassmann manifold were set to $\mathbf{M} = \mathbf{I}_{19 \times 3}$, $\mathbf{U} = \sigma^2 \mathbf{I}_{19}$, and $\mathbf{V} = \sigma^2 \mathbf{I}_3$, $\sigma = 0.3$, respectively. In addition, for the hyperparameters in methods other than GrCNF, please refer to Garcia Satorras et al. (2021).

Implementation The experimental hardware was built using a single NVIDIA A100 GPU with 80GB PCIe of GDDR6 RAM.

Table 5: Negative log-likelihood comparison on the test partition of DW4 dataset for different amounts of training samples; averaged over 3 runs and including standard deviations.

# of Samples	DW4			
	10 ²	10 ³	10 ⁴	10 ⁵
GNF	-2.30 ± 1.59	-7.04 ± 0.64	-7.19 ± 0.99	-7.93 ± 1.10
GNF-att	-2.02 ± 1.34	-4.13 ± 1.20	-5.25 ± 0.89	-6.74 ± 0.89
GNF-att-aug	-3.11 ± 2.15	-4.04 ± 3.40	-6.51 ± 0.49	-9.42 ± 1.15
Simple dynamics	-1.22 ± 0.05	-1.28 ± 0.01	-1.36 ± 0.02	-1.39 ± 0.04
E-NF	-0.54 ± 0.45	-9.89 ± 2.30	-12.15 ± 1.16	-15.29 ± 0.53
GrCNF	-12.53 ± 0.92	-13.74 ± 0.30	-14.09 ± 0.44	-16.07 ± 0.46

Table 6: Negative log-likelihood comparison on the test partition of LJ13 dataset for different amounts of training samples; averaged over 3 runs and including standard deviations.

# Samples	LJ13			
	10	10 ²	10 ³	10 ⁴
GNF	6.77 ± 0.39	-0.76 ± 1.12	-4.26 ± 2.76	-12.43 ± 1.21
GNF-att	6.91 ± 0.17	1.40 ± 0.79	-6.81 ± 2.09	-12.05 ± 2.28
GNF-att-aug	2.95 ± 0.55	-6.11 ± 1.12	-13.94 ± 0.95	-15.74 ± 0.58
Simple dynamics	-1.10 ± 2.55	-3.87 ± 0.25	-3.72 ± 0.08	-3.59 ± 0.52
E-NF	-12.86 ± 3.67	-15.75 ± 5.02	-31.51 ± 1.19	-32.83 ± 1.98
GrCNF	-23.64 ± 2.23	-44.24 ± 4.26	-58.02 ± 5.43	-58.71 ± 4.71

Table 7: Network architectures for QM9 Positional. (Left) GrCNF architecture, (Right) scale estimation architecture. The scale estimator estimates one scale parameter from each of the three orthonormal basis vectors $\mathbf{Y} = \{\mathbf{y}_i \in \mathbb{R}^{19}\}_{i=1}^3$, for $\sqrt{\Lambda} = \text{diag}(\{\sqrt{\lambda_i}\}_{i=1}^3)$ with three parameters $\{\sqrt{\lambda_i} \in \mathbb{R}\}_{i=1}^3$. Using the orthonormal orthogonal basis matrix \mathbf{Y} and the estimated scale parameter $\sqrt{\Lambda}$, we generate a point cloud $\mathbf{P} = \mathbf{Y}\sqrt{\Lambda}$. SiLU is an activation function proposed in (Ramachandran et al. (2017)) and BatchNorm. is a batch normalization layer in (Ioffe & Szegedy (2015)).

GrCNF for QM9 Positional			Scale Estimator for QM9 Positional		
Layer	Out Size	Norm./Act.	Layer	Out Size	Norm./Act.
Input	19×3	-	Input	19×3	-
HorP	19×3	-/Tanh	FC	128	BatchNorm./SiLU
Vec	57	-/-	FC	256	BatchNorm./SiLU
TW	32	-/Tanh	FC	256	BatchNorm./SiLU
TW	32	-/Tanh	FC	128	BatchNorm./SiLU
TW	32	-/Tanh	FC	3	-/ReLU
TW	1	-/Tanh			
HorL	19×3	-			

D Fundamentals of Concepts Associated with Grassmann Manifold

D.1 Definition of Stiefel Manifold

Definition 2. An (orthogonal or compact) Stiefel manifold $\text{St}(k, D)$ is defined as the set of orthonormal bases of k -dimensional subspaces in the Euclidean space \mathbb{R}^D as in (70).

$$\text{St}(k, D) := \{\mathbf{Y} \in \mathbb{R}^{D \times k} \mid \mathbf{Y}^\top \mathbf{Y} = \mathbf{I}_k\}. \quad (70)$$

For $\mathbf{Y} \in \text{St}(k, D)$, the space $\text{span}(\mathbf{Y})$ spanned by its column vectors is the element of $\text{Gr}(k, D)$.

$$f : \text{St}(k, D) \rightarrow \text{Gr}(k, D) : \mathbf{Y} \mapsto \text{span}(\mathbf{Y}). \quad (71)$$

$\text{St}(k, D)$ is a $Dk - \frac{k(k+1)}{2}$ -dimensional compact manifold (Absil et al. (2008)).

D.2 Equivalence Relation

To define the equivalence relation \sim ⁷ on a Stiefel manifold $\text{St}(k, D)$, we introduce the following two lemmas.

Lemma 1. The necessary and sufficient conditions for $\text{span}(\mathbf{Y}_1) = \text{span}(\mathbf{Y}_2)$ to hold for $\mathbf{Y}_1, \mathbf{Y}_2 \in \text{St}(k, D)$ are as follows.

$$\exists \mathbf{Q} \in \mathcal{O}(k) \text{ s.t. } \mathbf{Y}_2 = \mathbf{Y}_1 \mathbf{Q}. \quad (72)$$

Proof. $\text{span}(\mathbf{Y}_1) = \text{span}(\mathbf{Y}_2) \Leftarrow \mathbf{Y}_2 = \mathbf{Y}_1 \mathbf{Q}$. From the definition, $\mathbf{Y}_1^\top \mathbf{Y}_1 = \mathbf{Y}_2^\top \mathbf{Y}_2 = \mathbf{I}_k$, the following is obtained:

$$\mathbf{I}_k = \mathbf{Y}_1^\top \mathbf{Y}_1 = \mathbf{Q}^\top \mathbf{Y}_2^\top \mathbf{Y}_2 \mathbf{Q} = \mathbf{Q}^\top \mathbf{Q}. \quad (73)$$

Thus, there exists a k -dimensional orthogonal matrix $\mathbf{Q} \in \mathcal{O}(k)$. As the subspace $\text{span}(\mathbf{Y})$ is invariant to coordinate transformations by orthogonal matrices, $\text{span}(\mathbf{Y}_1) = \text{span}(\mathbf{Y}_2)$ is true.

$\text{span}(\mathbf{Y}_1) = \text{span}(\mathbf{Y}_2) \Rightarrow \mathbf{Y}_2 = \mathbf{Y}_1 \mathbf{Q}$. From the assumption, we immediately concluded that $\mathbf{Y}_2 = \mathbf{Y}_1 \mathbf{Q}$ for $\mathbf{Q} \in \mathcal{O}(k)$. \square

Lemma 2. We define the equivalence relation \sim on $\text{St}(k, D)$ to be $\mathbf{Y}_1 \sim \mathbf{Y}_2$ whenever (72) is satisfied with respect to $\mathbf{Y}_1, \mathbf{Y}_2 \in \text{St}(k, D)$. The fact that a binary relation is an equivalence relation \sim implies that the following three statements hold for $\forall \mathbf{Y}_1, \mathbf{Y}_2, \mathbf{Y}_3 \in \text{St}(k, D)$.

Reflexivity $\mathbf{Y}_1 \sim \mathbf{Y}_1$.

Symmetry $\mathbf{Y}_1 \sim \mathbf{Y}_2 \Rightarrow \mathbf{Y}_2 \sim \mathbf{Y}_1$.

Transitivity $\mathbf{Y}_1 \sim \mathbf{Y}_2 \wedge \mathbf{Y}_2 \sim \mathbf{Y}_3 \Rightarrow \mathbf{Y}_1 \sim \mathbf{Y}_3$.

Proof. With Lemma 1, we can confirm that it is valid as follows:

Reflexivity From $\mathbf{Y}_1 = \mathbf{Y}_1 \mathbf{I}$, $\mathbf{I} \in \mathcal{O}$, we obtain $\mathbf{Y}_1 \sim \mathbf{Y}_1$.

Symmetry As $\mathbf{Y}_2 = \mathbf{Y}_1 \mathbf{Q}$ is obtained from $\mathbf{Y}_1 \sim \mathbf{Y}_2$, and $\mathbf{Y}_2 \mathbf{Q}^\top = \mathbf{Y}_1$, $\mathbf{Q}^\top \in \mathcal{O}$ is true, then $\mathbf{Y}_2 \sim \mathbf{Y}_1$ is obtained.

Transitivity $\mathbf{Y}_3 = \mathbf{Y}_1 \mathbf{Q}_1 \mathbf{Q}_2$ with $\mathbf{Y}_2 = \mathbf{Y}_1 \mathbf{Q}_1$ and $\mathbf{Y}_3 = \mathbf{Y}_2 \mathbf{Q}_2$. $\mathbf{Q}_1 \mathbf{Q}_2$ is $(\mathbf{Q}_1 \mathbf{Q}_2)^\top (\mathbf{Q}_1 \mathbf{Q}_2) = \mathbf{Q}_2^\top \mathbf{Q}_1^\top \mathbf{Q}_1 \mathbf{Q}_2 = \mathbf{Q}_2^\top \mathbf{Q}_2 = \mathbf{I}$. Moreover, as $(\mathbf{Q}_1 \mathbf{Q}_2) (\mathbf{Q}_1 \mathbf{Q}_2)^\top = \mathbf{Q}_1 \mathbf{Q}_2 \mathbf{Q}_2^\top \mathbf{Q}_1^\top = \mathbf{I}$ holds, $\mathbf{Q}_1 \mathbf{Q}_2 \in \mathcal{O}$ is true. Therefore, we concluded $\mathbf{Y}_1 \sim \mathbf{Y}_3$. \square

The equivalence class of $\mathbf{Y} \in \text{St}(k, D)$ is denoted by $[\mathbf{Y}]$. In other words, $[\mathbf{Y}]$ is the set of all elements of $\text{St}(k, D)$ that are equivalent to \mathbf{Y} , and the equivalence relation on $\text{St}(k, D)$ divides $\text{St}(k, D)$ into equivalence classes with no intersection. Thus, \mathbf{Y} is then referred to as the representative of the equivalence class $[\mathbf{Y}]$. The set of equivalence classes is denoted $\text{St}(k, D)/\sim$ and is referred to as the

⁷Reflexive, symmetric and transitive binary relations. As a consequence of these properties, in a given set, one equivalence relation divides (classifies) the set into equivalence classes. Note that R is a binary relation in the set X if for any $x, y \in X$, only either x is related to y by the relation R , or x is not related to y based on the relation that R occurs. We write x is related to y by relation R as xRy .

quotient of $\text{St}(k, D)$ by the equivalence relation \sim . In addition, $\pi : \rightarrow \text{St}(k, D) \rightarrow \text{St}(k, D)/\sim$ is the natural projection that maps $\mathbf{Y} \in \text{St}(k, D)$ onto its equivalence class $[\mathbf{Y}]$. This projection π is surjection.

D.3 Quotient Manifold

Definition 3. Let $\overline{\mathcal{M}}$ be a manifold with equivalence relation \sim . The quotient space $\overline{\mathcal{M}}/\sim$ with \sim of $\overline{\mathcal{M}}$ is the set of all equivalence classes. Thus, $\overline{\mathcal{M}}/\sim := \{\pi(\overline{\mathbf{x}}) \mid \overline{\mathbf{x}} \in \overline{\mathcal{M}}\}$, where $\pi : \overline{\mathcal{M}} \rightarrow \overline{\mathcal{M}}/\sim$ is the natural projection and $\pi(\overline{\mathbf{x}}) := \{\overline{\mathbf{y}} \in \overline{\mathcal{M}} \mid \overline{\mathbf{y}} \sim \overline{\mathbf{x}}\}$. Then, $\overline{\mathcal{M}}$ is referred to as the total space or the total manifold. Moreover, $\overline{\mathcal{M}}/\sim$ is referred to as a quotient manifold of $\overline{\mathcal{M}}$ if $\overline{\mathcal{M}}/\sim$ admits a differentiable structure.

Let $\mathcal{M} = \overline{\mathcal{M}}/\sim$ be a quotient manifold. Further, suppose that $\overline{\mathcal{M}}$ is endowed with a Riemann metric \bar{g} , and let $\mathbf{x} = \pi(\mathbf{y})$. The horizontal space $T_{\overline{\mathbf{x}}}^h \overline{\mathcal{M}}$ is the orthogonal complement of the vertical space $T_{\overline{\mathbf{x}}}^v \overline{\mathcal{M}} := T_{\overline{\mathbf{x}}} \pi^{-1}(\mathbf{x})$ in the tangent space $T_{\overline{\mathbf{x}}} \overline{\mathcal{M}}$ and is defined as the follows:

$$T_{\overline{\mathbf{x}}}^h \overline{\mathcal{M}} := (T_{\overline{\mathbf{x}}}^v \overline{\mathcal{M}})^\perp = \{\bar{\boldsymbol{\eta}}_{\overline{\mathbf{x}}} \in T_{\overline{\mathbf{x}}} \overline{\mathcal{M}} \mid \bar{g}_{\overline{\mathbf{x}}}(\bar{\boldsymbol{\xi}}_{\overline{\mathbf{x}}}, \bar{\boldsymbol{\eta}}_{\overline{\mathbf{x}}}) = 0, \forall \bar{\boldsymbol{\xi}}_{\overline{\mathbf{x}}} \in T_{\overline{\mathbf{x}}}^v \overline{\mathcal{M}}\}. \quad (74)$$

The horizontal lift $\bar{\boldsymbol{\xi}}_{\overline{\mathbf{x}}}^h \in T_{\overline{\mathbf{x}}}^h \overline{\mathcal{M}}$ of the tangent vector $\boldsymbol{\xi}_{\mathbf{x}} \in T_{\mathbf{x}} \mathcal{M}$ at point $\overline{\mathbf{x}} \in \pi^{-1}(\mathbf{x})$ is a tangent vector that is uniquely determined as $d\pi_{\overline{\mathbf{x}}}(\bar{\boldsymbol{\xi}}_{\overline{\mathbf{x}}}^h) = \boldsymbol{\xi}_{\mathbf{x}}$ (Absil et al. (2008)).

D.4 Grassmann Manifold Exploiting the Quotient Structure

D.4.1 Tangent Space on $\text{St}(k, D)$

We describe the relationship between tangent space $T_{[\mathbf{Y}]} \text{Gr}(k, D)$ on $\text{Gr}(k, D)$ and tangent space $T_{\mathbf{Y}} \text{St}(k, D)$ on $\text{St}(k, D)$ to relate the tangent vectors of a Grassmann manifold $\text{Gr}(k, D)$ to the tangent vectors of a Stiefel manifold $\text{St}(k, D)$ in a matrix representation. We take the derivative on both sides of $\mathbf{Y}(t)^\top \mathbf{Y}(t) = \mathbf{I}_p$ in (70) by t and solve for $t = 0$.

$$\frac{d}{dt} \{ \mathbf{Y}(t)^\top \mathbf{Y}(t) \} = \frac{d}{dt} \mathbf{I}_p \quad (75)$$

$$\frac{d}{dt} \mathbf{Y}(t)^\top \mathbf{Y}(t) + \mathbf{Y}(t)^\top \frac{d}{dt} \mathbf{Y}(t) = 0 \quad (76)$$

$$\frac{d}{dt} \mathbf{Y}(0)^\top \mathbf{Y}(0) + \mathbf{Y}(0)^\top \frac{d}{dt} \mathbf{Y}(0) = 0 \quad (77)$$

$$\bar{\boldsymbol{\xi}}_{\mathbf{Y}}^\top \mathbf{Y} + \mathbf{Y}^\top \bar{\boldsymbol{\xi}}_{\mathbf{Y}} = 0. \quad (78)$$

where $\bar{\boldsymbol{\xi}}_{\mathbf{Y}} = \frac{d}{dt} \mathbf{Y}(0)$ is the tangent vector at \mathbf{Y} ⁸.

Definition 4. Define the tangent space $T_{\mathbf{Y}} \text{St}(k, D)$ at \mathbf{Y} on the Stiefel manifold as follows:

$$T_{\mathbf{Y}} \text{St}(k, D) = \left\{ \bar{\boldsymbol{\xi}}_{\mathbf{Y}} \in \mathbb{R}^{D \times k} \mid \bar{\boldsymbol{\xi}}_{\mathbf{Y}}^\top \mathbf{Y} + \mathbf{Y}^\top \bar{\boldsymbol{\xi}}_{\mathbf{Y}} = \mathbf{0}_k \right\}. \quad (79)$$

Let matrix $\mathbf{Y}_\perp \in \mathbb{R}^{D \times (D-k)}$ be a matrix satisfying the following:

$$\mathbf{Y}_\perp^\top \mathbf{Y}_\perp = \mathbf{I}_{D-k}, \quad \mathbf{Y}^\top \mathbf{Y}_\perp = 0, \quad \mathbf{Y} \mathbf{Y}^\top + \mathbf{Y}_\perp \mathbf{Y}_\perp^\top = \mathbf{I}_D. \quad (80)$$

As $[\mathbf{Y} \mathbf{Y}_\perp]$ is an orthogonal matrix⁹, the column vectors of \mathbf{Y} and \mathbf{Y}_\perp form an orthonormal basis in \mathbb{R}^D . Thus, any $D \times k$ matrix can be written in terms of the $\mathbf{C} \in \mathbb{R}^{k \times k}$ and $\mathbf{B} \in \mathbb{R}^{(D-k) \times k}$ coefficient matrices as follows:

$$\mathbf{Y} \mathbf{C} + \mathbf{Y}_\perp \mathbf{B}, \quad (81)$$

⁸The tangent space is defined independently for each point of the manifold; hence, the subscript \mathbf{Y} , as in $\bar{\boldsymbol{\xi}}_{\mathbf{Y}}$, is clearly stated to emphasize that it is a tangent vector at \mathbf{Y} .

⁹ $[\mathbf{Y} \mathbf{Y}_\perp]^{-1} [\mathbf{Y} \mathbf{Y}_\perp] = [\mathbf{Y} \mathbf{Y}_\perp]^\top [\mathbf{Y} \mathbf{Y}_\perp] = [\mathbf{Y} \mathbf{Y}_\perp] [\mathbf{Y} \mathbf{Y}_\perp]^\top = \mathbf{I}_D$.

where $\bar{\xi}_Y = YC + Y_\perp B$ is inserted. The following equation is obtained.

$$\bar{\xi}_Y^\top Y + Y^\top \bar{\xi}_Y = (YC + Y_\perp B)^\top Y + Y^\top (YC + Y_\perp B) \quad (82)$$

$$= B^\top Y_\perp^\top Y + C^\top Y^\top Y + Y^\top YC + Y^\top Y_\perp B \quad (83)$$

$$= B^\top Y^\top Y_\perp + C^\top + C \quad (84)$$

$$= C^\top + C \quad (85)$$

$$= \mathbf{0}_k. \quad (86)$$

Thus, the following equation is derived.

$$C^\top + C = \mathbf{0}_k. \quad (87)$$

Thus, C is a $k \times k$ skew-symmetric matrix $\text{Skew}(k)$. Therefore, we obtain the following as another representation of the tangent space on $\text{St}(k, D)$.

$$T_Y \text{St}(k, D) = \left\{ YC + Y_\perp B \mid C \in \text{Skew}(k), B \in \mathbb{R}^{(D-k) \times k} \right\}. \quad (88)$$

D.4.2 Riemannian Metric on $\text{St}(k, D)$

In the tangent space $T_x \mathcal{M}$ defined at each point $x \in \mathcal{M}$ on the manifold \mathcal{M} , the inner product h is endowed as a bilinear map. This h is referred to as a Riemannian metric on a manifold, and the manifold \mathcal{M} on which the Riemannian metric h is endowed is referred to as a Riemannian manifold (\mathcal{M}, h) . We define the Riemannian metric \bar{g} on $\text{St}(k, D)$ as follows.

$$\bar{g}_Y (\bar{\xi}_Y, \bar{\eta}_Y) := \text{tr} (\bar{\xi}_Y^\top \bar{\eta}_Y) \text{ s.t. } \bar{\xi}_Y, \bar{\eta}_Y \in T_Y \text{St}(k, D), Y \in \text{St}(k, D). \quad (89)$$

This is the standard inner product of $\mathbb{R}^{D \times k}$ induced by $T_Y \text{St}(k, D)$, with $T_Y \text{St}(k, D) \subset \mathbb{R}^{D \times k}$ ¹⁰.

D.4.3 Tangent Space on $\text{Gr}(k, D)$

We describe the relation between tangent spaces $T_{[Y]} \text{Gr}(k, D)$ and $T_Y \text{St}(k, D)$ to relate tangent vectors in tangent spaces $T_{[Y]} \text{Gr}(k, D)$ on $\text{Gr}(k, D)$ to tangent vectors $\bar{\xi}_Y \in T_Y \text{St}(k, D)$.

First, we define the vertical space $T_Y^v \text{St}(k, D)$ as a subspace of $T_Y \text{St}(k, D)$ as follows.

$$T_Y^v \text{St}(k, D) := T_Y \pi^{-1} ([Y]), \quad (90)$$

where $\pi : \text{St}(k, D) \rightarrow \text{Gr}(k, D)$ is the natural projection defined by $\pi(Y) = [Y]$ ¹². Thus, π converges all $Y' \in \text{St}(k, D)$ such that $Y \sim Y'$ to a point $[Y]$ on $\text{Gr}(k, D)$. Therefore, using (1), (90) can be transformed as follows.

$$T_Y^v \text{St}(k, D) = T_Y \{ YQ \mid Q \in \mathcal{O}(k) \}. \quad (91)$$

However, $\bar{\xi}_Y^v \in T_Y^v \text{St}(k, D)$ can be written as $\bar{\xi}_Y^v = YS$ with $S \in T_{I_k} \mathcal{O}(k)$.

$$T_{I_k} \mathcal{O}(k) = T_{I_k} \text{St}(k, k) \quad (92)$$

$$= \left\{ I_k C + (I_{k \perp} B = \mathbf{0}_k) \mid C \in \text{Skew}(k), B \in \mathbb{R}^{(k-k=0) \times k} \right\} \quad (93)$$

$$= \text{Skew}(k). \quad (94)$$

¹⁰The inner product $\mathbf{A} \cdot \mathbf{C} = \mathbf{A}^\top \mathbf{C}$ of a vector is typically referred to as the standard inner product. Further, matrices are similarly defined with a standard inner product, defined as $\mathbf{A} \cdot \mathbf{C} = \text{tr} (\mathbf{A}^\top \mathbf{C})$. A space $\mathbb{R}^{D \times k}$ such that the $D \times k$ matrix \mathbf{A} is an element is referred to as a matrix space. The standard basis of the matrix space can be constructed by a matrix wherein only one element in the matrix is 1 and the remaining are 0. The matrix space is a linear space because it satisfies the linearity that is similar to that in case of a linear vector space.

¹¹When \mathcal{N} is a submanifold of a Riemannian manifold (\mathcal{M}, g) , we define the Riemannian metric \bar{g} of \mathcal{N} to be:

$$\bar{g}_x (\xi, \eta) := g_x (\xi, \eta), \quad x \in \mathcal{N} \subset \mathcal{M}, \xi, \eta \in T_x \mathcal{N} \subset T_x \mathcal{M}.$$

\bar{g} is an induced metric and (\mathcal{N}, \bar{g}) is a Riemannian submanifold of (\mathcal{M}, g) . As $\text{St}(k, D)$ is a submanifold of $\mathbb{R}^{D \times k}$, we can define the standard inner product $\mathbf{A} \cdot \mathbf{C} = \text{tr} (\mathbf{A}^\top \mathbf{C})$ of $\mathbb{R}^{D \times k}$ as the induced metric \bar{g} . Thus, $\text{St}(k, D)$ is a Riemannian submanifold of $\mathbb{R}^{D \times k}$.

¹²Suppose a set is given a suitable equivalence relation. A natural projection is a map that sends each element of a set to the equivalence class to which it belongs.

Thus, we obtain the following formula.

$$T_{\mathbf{Y}}^v \text{St}(k, D) = \{\mathbf{Y}\mathbf{C} \mid \mathbf{C} \in \text{Skew}(k)\}. \quad (95)$$

Next, we define the horizontal space $T_{\mathbf{Y}}^h \text{St}(k, D)$ as the orthogonal complement of $T_{\mathbf{Y}}^v \text{St}(k, D)$ in $T_{\mathbf{Y}} \text{St}(k, D)$ endowed with the inner product (89).

$$T_{\mathbf{Y}}^h \text{St}(k, D) := (T_{\mathbf{Y}}^v \text{St}(k, D))^{\perp} \quad (96)$$

$$= \left\{ \bar{\xi}_{\mathbf{Y}}^h \in T_{\mathbf{Y}} \text{St}(k, D) \mid \text{tr} \left(\bar{\xi}_{\mathbf{Y}}^{h\top} \bar{\eta}_{\mathbf{Y}}^v \right) = 0, \bar{\eta}_{\mathbf{Y}}^v \in T_{\mathbf{Y}}^v \text{St}(k, D) \right\}. \quad (97)$$

Based on the fact that $T_{\mathbf{Y}}^v \text{St}(k, D)$ is a subspace of $T_{\mathbf{Y}} \text{St}(k, D)$ and $T_{\mathbf{Y}}^h \text{St}(k, D)$ is defined as its orthogonal complement, the direct sum decomposition is as follows.

$$T_{\mathbf{Y}} \text{St}(k, D) = T_{\mathbf{Y}}^v \text{St}(k, D) \oplus T_{\mathbf{Y}}^h \text{St}(k, D), \quad (98)$$

where \oplus denotes direct sum. Moreover, the tangent space is a linear space (Absil et al. (2008)). From (88), element $\mathbf{Y}\mathbf{C}$ of $T_{\mathbf{Y}}^v \text{St}(k, D)$ corresponds to the first term of (95); thus, (98) is formulated as follows:

$$T_{\mathbf{Y}}^h \text{St}(k, D) = \left\{ \bar{\xi}_{\mathbf{Y}}^h = \mathbf{Y}_{\perp} \mathbf{B} \mid \mathbf{B} \in \mathbb{R}^{(D-k) \times k} \right\}. \quad (99)$$

Note that the horizontal vector $\bar{\xi}_{\mathbf{Y}}^h$ is not necessarily an orthogonal matrix.

Finally, define the element $\bar{\xi}_{\mathbf{Y}}^h \in T_{\mathbf{Y}}^h \text{St}(k, D)$ of the horizontal space at $\mathbf{Y} \in \text{St}(k, D)$ for the tangent vector $\xi_{[\mathbf{Y}]} \in T_{[\mathbf{Y}]} \text{Gr}(k, D)$ at $[\mathbf{Y}] \in \text{Gr}(k, D)$ as satisfying the following formula.

$$d\pi(\mathbf{Y}) \left[\bar{\xi}_{\mathbf{Y}}^h \right] = \xi_{[\mathbf{Y}]}, \quad (100)$$

where $d\pi(\mathbf{Y}) : T_{\mathbf{Y}} \text{St}(k, D) \rightarrow T_{[\mathbf{Y}]} \text{Gr}(k, D)$ is the derivative $\frac{d\pi(\mathbf{Y})}{d\mathbf{Y}}$ of $\pi : \text{St}(k, D) \rightarrow \text{Gr}(k, D)$ at $\mathbf{Y} \in \text{St}(k, D)$. The $\bar{\xi}_{\mathbf{Y}}^h \in T_{\mathbf{Y}}^h \text{St}(k, D)$ is referred to as the horizontal lift at $\mathbf{Y} \in \text{St}(k, D)$ of $[\mathbf{Y}] \in \text{Gr}(k, D)$.

We describe the tangent space of $\text{Gr}(k, D)$ with the concept of horizontal lift.

Definition 5. Let $T_{\mathbf{Y}}^h \text{St}(k, D)$ be a horizontal space on $\text{St}(k, D)$. Then, we define the tangent space $T_{[\mathbf{Y}]} \text{Gr}(k, D)$ of the $\text{Gr}(k, D)$ as follows.

$$T_{[\mathbf{Y}]} \text{Gr}(k, D) = \left\{ \xi_{[\mathbf{Y}]} \mid d\pi(\mathbf{Y}) \left[\bar{\xi}_{\mathbf{Y}}^h \right] = \xi_{[\mathbf{Y}]}, \bar{\xi}_{\mathbf{Y}}^h \in T_{\mathbf{Y}}^h \text{St}(k, D) \right\}. \quad (101)$$

From the above, $\xi_{[\mathbf{Y}]} \in T_{[\mathbf{Y}]} \text{Gr}(k, D)$ is obtained from the map $d\pi(\mathbf{Y}) \left[\bar{\xi}_{\mathbf{Y}}^h \right]$ when $\bar{\xi}_{\mathbf{Y}}^h$ is obtained. The $\xi_{[\mathbf{Y}]}$ is defined by an equivalence class and cannot be treated numerically in matrix form; however, it is sufficient to obtain the $\bar{\xi}_{\mathbf{Y}}^h$ for actual numerical calculations. For $\xi_{[\mathbf{Y}]} \in T_{[\mathbf{Y}]} \text{Gr}(k, D)$, there exists a $\bar{\xi}_{\mathbf{Y}}^h \in T_{\mathbf{Y}}^h \text{St}(k, D)$ that uniquely satisfies (100). In other words, we can handle it in matrix form by using elements of the horizontal space of Stiefel manifolds through the concept of horizontal lifting. Figure 1 is a conceptual diagram of the tangent space representation of a Grassmann manifold by horizontal lift.

D.4.4 Riemannian Metric on $\text{Gr}(k, D)$

We define the Riemannian metric g of $\text{Gr}(k, D)$ through the concept of horizontal lift.

Definition 6. Let $\bar{\xi}_{\mathbf{Y}}^h$ and $\bar{\eta}_{\mathbf{Y}}^h$ be the horizontal lifts that become $d\pi(\mathbf{Y}) \left[\bar{\xi}_{\mathbf{Y}}^h \right] = \xi_{[\mathbf{Y}]}$ and $d\pi(\mathbf{Y}) \left[\bar{\eta}_{\mathbf{Y}}^h \right] = \eta_{[\mathbf{Y}]}$, respectively. Then, we define the Riemannian metric on $\text{Gr}(k, D)$ as follows:

$$g_{[\mathbf{Y}]} (\xi_{[\mathbf{Y}]}, \eta_{[\mathbf{Y}]}) := \bar{g}_{\mathbf{Y}} \left(\bar{\xi}_{\mathbf{Y}}^h, \bar{\eta}_{\mathbf{Y}}^h \right) = \text{tr} (\mathbf{B}^{\top} \mathbf{D}), \quad (102)$$

where \mathbf{B} and \mathbf{D} are matrices that are $\bar{\xi}_{\mathbf{Y}}^h = \mathbf{Y}_{\perp} \mathbf{B}$ and $\bar{\eta}_{\mathbf{Y}}^h = \mathbf{Y}_{\perp} \mathbf{D}$, respectively.

D.5 Invariant Measures

Let the column vectors of matrix $\mathbf{Y} = \{\mathbf{y}_1, \dots, \mathbf{y}_k\} \in \mathbb{R}^{D \times k}$ be the orthonormal basis that span the subspace $\text{span}(\mathbf{Y}) \in \text{Gr}(k, D)$ in \mathbb{R}^D , and the column vectors of $\mathbf{Y}_\perp = \{\mathbf{y}_{k+1}, \dots, \mathbf{y}_D\} \in \mathbb{R}^{D \times D-k}$ be the orthogonal complementary space $\text{span}(\mathbf{Y}_\perp)$ of $\text{span}(\mathbf{Y})$, respectively. Then, the following differential form can be defined.

$$(d\mathbf{Y}) = \bigwedge_{j=1}^{D-k} \bigwedge_{i=1}^k \mathbf{y}_{k+j}^\top d\mathbf{y}_i \quad (103)$$

$$= (\mathbf{y}_{k+1}^\top d\mathbf{y}_1 \wedge \dots \wedge \mathbf{y}_{k+1}^\top d\mathbf{y}_k) \wedge \dots \wedge (\mathbf{y}_D^\top d\mathbf{y}_1 \wedge \dots \wedge \mathbf{y}_D^\top d\mathbf{y}_k). \quad (104)$$

where \wedge is the wedge product and the relation satisfies $\omega_i \wedge \omega_i = \omega_j \wedge \omega_j = 0$ and $\omega_i \wedge \omega_j = -\omega_j \wedge \omega_i$. The above equation is in $k(D-k)$ -order differential form, which is an invariant measure on $\text{Gr}(k, D)$ (Chikuse (2003)).

If we define the matrix \mathbf{X}_\perp to be $[\mathbf{X} \ \mathbf{X}_\perp]$ for any point $\mathbf{X} = \{\mathbf{x}_1, \dots, \mathbf{x}_k\} \in \text{St}(k, D)$, the differential form for an invariant measure on $\text{St}(k, D)$ is defined as follows.

$$(d\mathbf{X}) = \bigwedge_{j=1}^{D-k} \bigwedge_{i=1}^k \mathbf{x}_{k+j}^\top d\mathbf{x}_i \bigwedge_{i < j}^k \mathbf{x}_j^\top d\mathbf{x}_i = (d\mathbf{Y}) (d\mathbf{Q}), \quad (105)$$

where $(d\mathbf{Q})$ is the invariant measure of $\mathcal{O}(k)$. The integral of (105), that is, the volume of $\text{St}(k, D)$, can be evaluated as follows:

$$V_{\text{St}(k, D)} = \int_{\text{St}(k, D)} (d\mathbf{X}). \quad (106)$$

(106) can be computed as follows. First, the surface S_D of the D -dimensional unit sphere can be defined as follows:

$$S_D = \frac{d}{dr} \Big|_{r=1} V_D = DV_D = \frac{D\pi^{\frac{D}{2}}}{\Gamma\left(\frac{D}{2} + 1\right)} = \frac{2\pi^{\frac{D}{2}}}{\Gamma\left(\frac{D}{2}\right)}, \quad (107)$$

where V_D is the volume of a D -dimensional sphere $\frac{\pi^{\frac{D}{2}}}{\Gamma\left(\frac{D}{2} + 1\right)} r^D$ and $\Gamma\left(\frac{D}{2}\right)$ is the gamma function. Then, the following equation is obtained.

$$\int_{\text{St}(k, D)} (d\mathbf{X}) = S_D \int_{\text{St}(k-1, D-1)} (d\mathbf{X}_1), \quad (108)$$

where $(d\mathbf{X}_1)$ is the differential form of $\text{St}(k-1, D-1)$. Thus, (106) can be transformed as follows.

$$V_{\text{St}(k, D)} = \int_{\text{St}(k, D)} (d\mathbf{X}) = \prod_{i=1}^k S_D = \frac{2^k \pi^{\frac{Dk}{2}}}{\Gamma_k\left(\frac{D}{2}\right)}, \quad (109)$$

where $\Gamma_k\left(\frac{D}{2}\right)$ is the multidimensional gamma function. The invariant measure $(d\mathbf{X})$ is an unnormalized measure. A measure normalized to be a probability measure can be formulated as follows:

$$[d\mathbf{X}] = \frac{1}{V_{\text{St}(k, D)}} (d\mathbf{X}). \quad (110)$$

This is a uniform distribution on $\text{St}(k, D)$. As $\text{St}(k, k) = \mathcal{O}(k)$, the volume $V_{\mathcal{O}(k)}$ of $\mathcal{O}(k)$ can be represented using $(d\mathbf{Q})$ as follows.

$$V_{\mathcal{O}(k)} = V_{\text{St}(k, k)} = \frac{2^k \pi^{\frac{k^2}{2}}}{\Gamma_k\left(\frac{k}{2}\right)}. \quad (111)$$

Furthermore, a measure normalized to be a probability measure can be represented by the following:

$$[d\mathbf{Q}] = \frac{1}{V_{\mathcal{O}(k)}} (d\mathbf{Q}). \quad (112)$$

From the above, the probability density function $U_{\mathcal{O}(k)}(\mathbf{Q})$ of the uniform distribution on $\mathcal{O}(k)$ is as follows:

$$U_{\mathcal{O}(k)}(\mathbf{Q}) = \frac{1}{V_{\mathcal{O}(k)}} \text{ s.t. } \mathbf{Q} \in \mathcal{O}(k), \quad (113)$$

$$\int_{\mathcal{O}(k)} U_{\mathcal{O}(k)}(\mathbf{Q}) (d\mathbf{Q}) = \int_{\mathcal{O}(k)} \frac{1}{V_{\mathcal{O}(k)}} (d\mathbf{Q}) = \int_{\mathcal{O}(k)} [d\mathbf{Q}] = 1. \quad (114)$$

As $\text{Gr}(k, D)$ is defined as a quotient manifold $\text{St}(k, D) / \mathcal{O}(k)$ as in (2), the volume $V_{\text{Gr}(k, D)}$ of $\text{Gr}(k, D)$ can be defined as follows.

$$V_{\text{Gr}(k, D)} = \int_{\text{Gr}(k, D)} (d\mathbf{Y}) = \frac{V_{\text{St}(k, D)}}{V_{\mathcal{O}(k)}} = \frac{V_{\text{St}(k, D)}}{V_{\text{St}(k, k)}} = \frac{\pi^{\frac{k(D-k)}{2}} \Gamma_k(\frac{k}{2})}{\Gamma_k(\frac{D}{2})}. \quad (115)$$

The measure normalized to be a probability measure is expressed as:

$$[d\mathbf{Y}] = \frac{1}{V_{\text{Gr}(k, D)}} (d\mathbf{Y}). \quad (116)$$

D.6 Retraction

In general, the points except the origin ($\mathbf{p}(0) = \mathbf{x}$) of the tangent space $T_{\mathbf{x}}\mathcal{M}$ at \mathbf{x} on the manifold \mathcal{M} are not elements on \mathcal{M} ($\mathbf{p}(t) \in T_{\mathbf{x}}\mathcal{M}, t \neq 0$). Therefore, if the result of the operation on the tangent space is to be used at another point on the manifold \mathcal{M} , it is necessary to map $\mathbf{p}(t)$ to the manifold \mathcal{M} . The map from a tangent space to a manifold is referred to as an exponential map. However, because the exponential map is computationally expensive, retraction based on numerical linear algebra is often used as an alternative (Zhu & Sato (2021)). Retraction is a method for approximating an exponential map to first order while maintaining global convergence in optimization algorithms on Riemannian manifolds. The most commonly used retractions on $\text{Gr}(k, D)$ are methods based on QR decomposition or singular-value decomposition (SVD) (Absil et al. (2008); Zhu & Sato (2021)). In addition, a retraction based on the Cayley transform is introduced in Zhu & Sato (2021). This retraction is closely related to the Cayley transform on $\text{St}(k, D)$ (Wen & Yin (2013); Xiaojing (2017); Zhu & Duan (2019)) and the Projected polynomial retraction (Gawlik & Leok (2018a)).

D.6.1 Exponential Map and Retraction

Geodesics on $\text{Gr}(k, D)$ can be expressed as the equivalence class $[\exp_{\mathbf{Y}}^{\text{Gr}}(t\bar{\xi}_{\mathbf{Y}})]$, where

$$\exp_{\mathbf{Y}}^{\text{Gr}}(t\bar{\xi}_{\mathbf{Y}}) = [\mathbf{Y} \quad \mathbf{Y}_{\perp}] \exp(t\mathfrak{B}) \mathbf{I}_{D \times k}. \quad (117)$$

Here, \exp on the right-hand side is the matrix exponential, and $\mathfrak{B} = \begin{bmatrix} \mathbf{0}_k & -\mathbf{B}^{\top} \\ \mathbf{B} & \mathbf{0}_{D-k} \end{bmatrix} \in \text{skew}(D)$, where \mathbf{B} satisfies $\bar{\xi}_{\mathbf{Y}} = \mathbf{Y}_{\perp} \mathbf{B}$. We can use a following exponential map that is mathematically equivalent to (117) (Edelman et al. (1998)):

$$\exp_{\mathbf{Y}}^{\text{Gr}}(t\bar{\xi}_{\mathbf{Y}}) := \{\mathbf{Y}\mathbf{V} \cos(\Sigma t) + \mathbf{U} \sin(\Sigma t)\} \mathbf{V}^{\top}, \quad (118)$$

where $\mathbf{U}, \Sigma, \mathbf{V}^{\top} = \text{SVD}(\bar{\xi}_{\mathbf{Y}})$.

Further, we can use the Padé approximation to approximate geodesics on Grassmann manifolds as follows:

$$\mathbf{Y}(t) = [\mathbf{Y} \quad \mathbf{Y}_{\perp}] r_m(t\mathfrak{B}) \mathbf{I}_{D \times k} \approx \exp_{\mathbf{Y}}^{\text{Gr}}(t\bar{\xi}_{\mathbf{Y}}), \quad (119)$$

where $r_m(\mathbf{X})$ is the m th-order diagonal Padé approximation to the matrix exponential $\exp(\mathbf{X})$. See the expression of $r_m(\mathbf{X})$ in Moler & Loan (2003). The simplest member of this class is surely the first-order Padé approximation

$$\bar{R}_{\mathbf{Y}}(t\bar{\xi}_{\mathbf{Y}}) := [\mathbf{Y} \quad \mathbf{Y}_{\perp}] r_1(t\mathfrak{B}) \mathbf{I}_{D \times k} \quad (120)$$

$$= [\mathbf{Y} \quad \mathbf{Y}_{\perp}] \left(I_n - \frac{t}{2} \mathfrak{B} \right)^{-1} \left(\mathbf{I}_D + \frac{t}{2} \mathfrak{B} \right) \mathbf{I}_{D \times k}, \quad (121)$$

which is also known as the Cayley transform. From the error expression $\exp(\mathbf{Y}) = r_m(\mathbf{Y}) + O(\|\mathbf{Y}\|^{2m+1})$ of the Padé approximation, we have

$$\bar{R}_{\mathbf{Y}}(t\bar{\xi}_{\mathbf{Y}}) = \exp_{\mathbf{Y}}^{\text{Gr}}(t\bar{\xi}_{\mathbf{Y}}) + O\left(t^{2m+1} \|\bar{\xi}_{\mathbf{Y}}\|^{2m+1}\right) \quad (122)$$

which is also given by Theorem 3 in Gawlik & Leok (2018b).

D.6.2 Horizontal Retraction

From Definition 3 in Zhu & Sato (2021), (121) is a horizontal retraction, and

$$R_{[\mathbf{Y}]}(t\bar{\xi}_{[\mathbf{Y}]}) := \left[\bar{R}_{\mathbf{Y}}(t\bar{\xi}_{\mathbf{Y}}^h) \right] \quad (123)$$

is a retraction on $\text{Gr}(k, D)$ as a quotient manifold defined by (2). This is because \bar{R} satisfies the invariance condition that $\bar{R}_{\mathbf{Y}}(t\bar{\xi}_{\mathbf{Y}}^h) \sim \bar{R}_{\mathbf{Y}'}(t\bar{\xi}_{\mathbf{Y}'}^h)$ for all $\mathbf{Y} \in \text{St}(k, D)$, $\mathbf{Y}' \in \text{St}(k, D)$, $\bar{\xi}_{\mathbf{Y}} \in T_{\mathbf{Y}}^h \text{St}(k, D)$ and $\bar{\xi}_{\mathbf{Y}'} \in T_{\mathbf{Y}'}^h \text{St}(k, D)$ such that $\mathbf{Y} \sim \mathbf{Y}'$ and $\bar{\xi}_{\mathbf{Y}}$ and $\bar{\xi}_{\mathbf{Y}'}$ are horizontal lifts of $\xi_{[\mathbf{Y}]} \in T_{[\mathbf{Y}]} \text{Gr}(k, D)$ at \mathbf{Y} and \mathbf{Y}' , respectively.

In low-rank cases, we can obtain an economical version of (121) as follows (Zhu & Sato (2021)).

$$\bar{R}_{\mathbf{Y}}(t\bar{\xi}_{\mathbf{Y}}^h) = \mathbf{Y} + t\bar{\xi}_{\mathbf{Y}}^h - \left(\frac{t^2}{2}\mathbf{Y} + \frac{t^3}{4}\bar{\xi}_{\mathbf{Y}}^h \right) \left(\mathbf{I}_k + \frac{t^2}{4}\bar{\xi}_{\mathbf{Y}}^{h\top}\bar{\xi}_{\mathbf{Y}}^h \right)^{-1} \bar{\xi}_{\mathbf{Y}}^{h\top}\bar{\xi}_{\mathbf{Y}}^h. \quad (124)$$

The inverse retraction $\left(\bar{R}_{[\mathbf{Y}]}^{-1} \right)_{\mathbf{Y}}^h : \text{St}(k, D) \rightarrow T_{\mathbf{Y}}^h \text{St}(k, D)$ of $\bar{R}_{\mathbf{Y}}(t\bar{\xi}_{\mathbf{Y}}^h)$ is the following:

$$\left(\bar{R}_{[\mathbf{Y}]}^{-1}([\mathbf{X}]) \right)_{\mathbf{Y}}^h = \bar{R}_{\mathbf{Y}}^{-1}(\mathbf{X}) \quad (125)$$

$$= 2\mathbf{Y}_{\perp}\mathbf{Y}_{\perp}^{\top}\mathbf{X} (\mathbf{I}_k + \mathbf{Y}^{\top}\mathbf{X})^{-1} = 2(\mathbf{X} - \mathbf{Y}\mathbf{Y}^{\top}\mathbf{X})(\mathbf{I}_k + \mathbf{Y}^{\top}\mathbf{X})^{-1}. \quad (126)$$